

COMBINATORIAL THEORY OF THE SEMICLASSICAL EVALUATION OF TRANSPORT MOMENTS I: EQUIVALENCE WITH THE RANDOM MATRIX APPROACH

G. BERKOLAIKO AND J. KUIPERS

ABSTRACT. To study electronic transport through chaotic quantum dots, there are two main theoretical approaches. One involves substituting the quantum system with a random scattering matrix and performing appropriate ensemble averaging. The other treats the transport in the semiclassical approximation and studies correlations among sets of classical trajectories. There are established evaluation procedures within the semiclassical evaluation that, for several linear and non-linear transport moments to which they were applied, have always resulted in the agreement with random matrix predictions. We prove that this agreement is universal: any semiclassical evaluation within the accepted procedures is equivalent to the evaluation within random matrix theory.

The equivalence is shown by developing a combinatorial interpretation of the trajectory sets as ribbon graphs (maps) with certain properties and exhibiting systematic cancellations among their contributions. Remaining trajectory sets can be identified with primitive (palindromic) factorisations whose number gives the coefficients in the corresponding expansion of the moments of random matrices. The equivalence is proved for systems with and without time reversal symmetry.

1. INTRODUCTION

Transport through a chaotic cavity is usually studied through a scattering description. For a chaotic cavity attached to two leads with N_1 and N_2 channels respectively, the scattering matrix is an $N \times N$ unitary matrix, where $N = N_1 + N_2$. It can be separated into transmission and reflection subblocks

$$(1) \quad S(E) = \begin{pmatrix} \mathbf{r} & \mathbf{t}' \\ \mathbf{t} & \mathbf{r}' \end{pmatrix},$$

which encode the dynamics of the system and the relation between the incoming and outgoing wavefunctions in the leads. The transport statistics of the cavity in question can now be expressed in terms of the subblocks of $S(E)$. For example, the conductance is proportional to the trace $\text{Tr} [\mathbf{t}^\dagger \mathbf{t}]$ (Landauer-Büttiker formula [19, 32, 33]), while other physical properties are expressible through higher moments like $\text{Tr} [\mathbf{t}^\dagger \mathbf{t}]^n$.

There are two main approaches to studying the transport statistics in clean ballistic systems: a random matrix theory (RMT) approach, which argues that S can be viewed as a random matrix from a suitable ensemble, and a semiclassical approach that approximates elements of the matrix S by sums over open scattering trajectories through the cavity.

It was shown by Blümel and Smilansky [12, 13] that the scattering matrix of a chaotic cavity is well modelled by the Dyson's circular ensemble of random matrices of suitable symmetry. Thus, transport properties of chaotic cavities are often treated by replacing the scattering matrix with a random one (see [2] for a review). Calculating the averages over the appropriate random

matrix ensemble is a very active area with many different approaches. A partial list of recent results include the papers [28, 34, 42, 44, 53, 57, 58, 63, 64, 74]. In Section 2 we review some basic facts about integration over random matrices.

On the other hand, the semiclassical approach makes use of the following approximation for the scattering matrix elements [45, 60, 61]

$$(2) \quad S_{oi}(E) \approx \frac{1}{\sqrt{N\tau_d}} \sum_{\gamma(i \rightarrow o)} A_\gamma(E) e^{\frac{i}{\hbar} S_\gamma(E)},$$

which involves the open trajectories γ which start in channel i (for “input”) and end in channel o (for “output”), with their action S_γ and stability amplitude A_γ . The prefactor also involves τ_d which is the average dwell time, or time trajectories spend inside the cavity. For transport moments one considers quantities of the type

$$(3) \quad M_n(X) = \left\langle \text{Tr} [X^\dagger X]^n \right\rangle_E \sim \left\langle \frac{1}{(N\tau_d)^n} \sum_{i_j, o_j} \sum_{\substack{\gamma_j(i_j \rightarrow o_j) \\ \gamma'_j(i_{j+1} \rightarrow o_j)}} \prod_{j=1}^n A_{\gamma_j} A_{\gamma'_j}^* e^{\frac{i}{\hbar} (S_{\gamma_j} - S_{\gamma'_j})} \right\rangle,$$

where the trace means we identify $i_{n+1} = i_1$ and where X is either the transmitting or the reflecting subblock of the scattering matrix. The averaging is performed over a window of energies E which is classically small but semiclassically large: the width ΔE of the window satisfies $\hbar/N\tau_d \ll \Delta E \ll E$. Note that we use dagger to mean conjugate-transpose of a matrix and star to denote complex conjugation.

The choice of the subblock X affects the sums over the possible incoming and outgoing channels, but not the trajectory structure which involves $2n$ classical trajectories connecting channels. Of these, n trajectories γ_j , $j = 1, \dots, n$, contribute with positive action while n trajectories γ'_j contribute with negative action. In the semiclassical limit of $\hbar \rightarrow 0$ we require that these sums approximately cancel on the scale of \hbar so that the corresponding trajectories can contribute consistently when we apply the averaging in (3).

The semiclassical treatment will be reviewed in Section 3. The main idea of the treatment is that, in order to achieve a small action difference, the trajectories $\{\gamma'_j\}$, must follow the path of trajectories $\{\gamma_j\}$ most of the time, deviating only in small regions called *encounters*. The topological configuration of encounters and trajectories’ stretches between them is described using a *diagram*. The task of semiclassical evaluation thus splits into two parts: evaluation of the contribution of a given diagram by integrating over all possible trajectories of given structure and enumerating all possible diagrams.

For the former task, a well established approximation emerged by extending the pioneering work of Richter and Sieber [61] by a group of physicists based mainly in Essen: S. Müller, S. Heusler, P. Braun and F. Haake, [25, 47]. Henceforth we refer to this approximation as the “Essen ansatz”. Roughly speaking, it assigns to each diagram a weight which depends on the number and type of encounters and the number of trajectory stretches between the encounters. The approximation is derived based on physically justified assumptions; a mathematical derivation remains outside reach even for the simplest chaotic systems.

This approach to quantum transport was founded on the earlier semiclassical treatment of the two-point correlator of spectral densities of closed systems. There, correlations between pairs of periodic orbits [11, 23, 48, 49, 66] or sets of pseudo-orbits [24, 46] could be shown to be responsible for the universal behaviour in line with RMT. In fact a one-to-one mapping exists

between the semiclassical diagrams and those that arise in a perturbative expansion of the σ model and hence the equivalence between semiclassics and RMT established [46, 49]. The full equivalence for arbitrary correlators is yet to be demonstrated however.

Returning to transport through open systems, within the Essen ansatz incremental progress has been made in evaluating various transport-related quantities, see for example [4, 6, 7, 14, 25, 29, 31, 47, 61]. Interestingly, transport diagrams can be related to the closed periodic orbit pairs of spectral statistics by connecting the outgoing and incoming channels (possibly with additional encounters introduced). Reversing the process, transport diagrams may be generated by cutting periodic orbits and this approach has been employed to derive the first two moments [14, 25, 47]. For higher moments this procedure becomes more involved, though it does lead to interesting combinatorial problems [54, 55]. Alternatively, transport diagrams can be generated without recourse to periodic orbits leading to a perturbative expansion of moment generating functions for several orders in the parameter $1/N$ [4, 7, 9]. Here instead we develop a combinatorial approach to directly describe all transport diagrams.

For the transport moments that have been evaluated semiclassically, in every case where a RMT prediction was available it was found to be in full agreement with the semiclassical evaluation. This paper is devoted to proving a general theorem that implies that this will always remain the case: *any* semiclassical evaluation within the Essen ansatz is *equivalent* to the RMT evaluation.

Before we formulate our theorem, we note that the trace of any form can be expanded as a sum of products of matrix elements. For example, the trace in equation (3) expands as

$$\begin{aligned}
 (4) \quad \text{Tr} \left[X^\dagger X \right]^n &= \sum_{i_j, o_j} S_{i_1, o_n}^\dagger S_{o_n, i_n} \cdots S_{o_2, i_2} S_{i_2, o_1}^\dagger S_{o_1, i_1} \\
 &= \sum_{i_j, o_j} S_{o_n, i_n} \cdots S_{o_2, i_2} S_{o_1, i_1} S_{o_n, i_1}^* \cdots S_{o_2, i_3}^* S_{o_1, i_2}^* \\
 &= \sum_{i_j, o_j} Z_{i_1, o_1} Z_{i_2, o_2} \cdots Z_{i_n, o_n} Z_{i_2, o_1}^* Z_{i_3, o_2}^* \cdots Z_{i_1, o_n}^*
 \end{aligned}$$

where X is a sub-block of the scattering matrix S , the variables i_1, \dots, i_n run over all columns of S that appear in X and the variables o_1, \dots, o_n run over all rows of S in X . In the last line we switched from the matrix S to its transpose $Z = S^T$ as this will make further notation less confusing. From equation (4) it is clear that if we can evaluate the averages of products of matrix elements of S (or Z), we can have access to every linear transport moment. The same goes for the nonlinear transport moments, i.e. averages of the form $\langle \text{Tr} [X^\dagger X]^{n_1} \text{Tr} [X^\dagger X]^{n_2} \cdots \rangle$.

Theorem 1.1. *Within the Essen ansatz, the energy average of a product of the elements of the scattering matrix $S(E)$ (or $Z(E) = S^T(E)$) coincides with the corresponding average in RMT,*

$$(5) \quad C_E(\mathbf{a}, \mathbf{b}) \equiv \langle Z_{a_1 a_{\bar{1}}} \cdots Z_{a_s a_{\bar{s}}} Z_{b_1 b_{\bar{1}}}^* \cdots Z_{b_t b_{\bar{t}}}^* \rangle_E = \langle U_{a_1 a_{\bar{1}}} \cdots U_{a_s a_{\bar{s}}} U_{b_1 b_{\bar{1}}}^* \cdots U_{b_t b_{\bar{t}}}^* \rangle_{\text{RMT}}.$$

For scattering matrices with time-reversal symmetry the appropriate RMT average is over Circular Orthogonal Ensemble; without the symmetry the RMT average is over Circular Unitary Ensemble.

We emphasize that equality (5) is established to all orders in $1/N$, the usual expansion parameter of the quantities involved.

To prove Theorem 1.1 we will put the diagrammatic method of the semiclassical approximation on a more rigorous footing, carefully describing diagrams as ribbon graphs with certain colorability properties. We define operations on the diagrams that lead to cancellations and, eventually, to the equivalence with the RMT calculation.

We note that a preliminary outline of this theorem was published in [8]. While in the process of writing up, we were notified by Marcel Novaes that he achieved a similar breakthrough although only for systems without time-reversal symmetry. His original approach uses a combinatorial identity that remains unproved [54, 55], but a new approach provides the complete equivalence using a semiclassical matrix model [56].

It is important to mention that Theorem 1.1 does not produce any new formulae for moments such as $M_n(X)$, it only establishes the equivalence of the two existing approaches to their evaluation. However, the description of the diagrams that we develop in the proof can be analyzed further to yield new results. This is done in the second part of this work [9], where we formalize the semiclassical evaluation of moments, re-cast it as a summation over factorizations of given permutations, and thus calculate $M_n(X)$ for any n to several orders in the small parameter $1/N$.

The layout of the paper is as follows: in sections 2 and 3 we review the relevant notions and results from random matrix theory and semiclassical approximation, correspondingly. Section 4 discusses general properties of the sets of trajectories contributing on the semiclassical side. In section 5 and 6 we define and study the diagrams that classify contributing sets of orbits and relate them to the random matrix expansions for Circular Unitary and Orthogonal Ensembles, correspondingly. We endeavored to make the paper readable to a wide variety of audiences, providing numerous examples and figures to illustrate the discussed concepts.

2. RMT PREDICTION

It has been argued [12, 13] that scattering through a chaotic cavity is described by a unitary matrix from an appropriate random matrix ensemble. In the absence of Time Reversal Symmetry (TRS) the Circular Unitary Ensemble (CUE) is used. If TRS is present the appropriate ensemble is the Circular Orthogonal Ensemble (COE). The final classical symmetry class involves particles with spin $\frac{1}{2}$, for which breaking spin-rotation symmetry through spin-orbit interactions while retaining TRS leads to the Circular Symplectic Ensemble (CSE).

The CUE is the unitary group $U(N)$ endowed with the Haar measure. The averages of products of the elements of matrices $U \in U(N)$ have been studied in [15, 38, 62, 78] among other works. The main result is

$$(6) \quad \langle U_{a_1 a_{\bar{1}}} \dots U_{a_s a_{\bar{s}}} U_{b_1 b_{\bar{1}}}^* \dots U_{b_t b_{\bar{t}}}^* \rangle_{\text{CUE}(N)} = \delta_{t,s} \sum_{\sigma, \pi \in S_t} V_N^U(\sigma^{-1}\pi) \prod_{k=1}^t \delta(a_k - b_{\sigma(k)}) \delta\left(a_{\bar{k}} - b_{\pi(k)}\right),$$

where S_t is the symmetric group of permutations of the set $\{1, \dots, t\}$, $\delta_{k,n} = \delta(k-n)$ is the Kronecker delta (the latter notation is used solely to avoid nesting subindices) and the coefficient $V_N^U(\sigma^{-1}\pi)$ depends only on the lengths of cycles in the cycle expansion of $\sigma^{-1}\pi$, i.e. on the conjugacy class of the permutation $\sigma^{-1}\pi$. For this reason we will refer to V_N^U as the CUE class coefficients.¹

¹Another name present in the literature is ‘‘Weingarten’’ function [78], even though it was probably Samuel [62] who first defined the function and systematically studied it.

The COE is the ensemble of *unitary symmetric matrices*² with a probability distribution obtained from the CUE through the mapping $W = UU^T$, where U is a unitary matrix from the CUE and U^T its transpose. The result analogous to (6) reads [15] (see also [39]),

$$(7) \quad \langle W_{a_1 a_{\bar{1}}} \cdots W_{a_s a_{\bar{s}}} W_{b_1 b_{\bar{1}}}^* \cdots W_{b_t b_{\bar{t}}}^* \rangle_{\text{COE}(N)} = \delta_{t,s} \sum_{\pi \in S_{2t}} V_N^{\text{O}}(\pi) \prod_{z \in Z_t} \delta(a_z - b_{\pi(z)}),$$

where π is a permutation on the set $Z_t = \{1, \dots, t, \bar{t}, \dots, \bar{1}\}$.

We mention that averaging formulae similar to (6) and (7) have recently become available for a much bigger variety of random matrix ensembles, see [36] and references therein.

Both types of class coefficients used above can be calculated recursively. Namely, the class coefficients V_N^{U} were derived by Samuel [62] to satisfy $V_N^{\text{U}}(\emptyset) = 1$ and

$$(8) \quad NV_N^{\text{U}}(c_1, \dots, c_k) + \sum_{p+q=c_1} V_N^{\text{U}}(p, q, c_2, \dots, c_k) + \sum_{j=2}^k c_j V_N^{\text{U}}(c_1 + c_j, \dots, \hat{c}_j, \dots, c_k) \\ = \delta_{c_1,1} V_N^{\text{U}}(c_2, \dots, c_k).$$

Here c_1, \dots, c_k are the lengths of the cycles in the cycle expansion of $\sigma^{-1}\pi$. The notation \hat{c}_j means that the element c_j has been removed from the list. Finally, $\delta_{c_1,1}$ is the Kronecker delta.

The corresponding recursion relation for the COE class coefficients were derived by Brouwer and Beenakker [15]. They represent the permutation π in equation (7) as the product

$$(9) \quad \pi = T' \pi_e \pi_o T'',$$

where T' and T'' are some involutions satisfying $T'(j) = j$ or \bar{j} , π_o is a permutation on the set $\{1, \dots, t\}$ and π_e is a permutation on the set $\{\bar{t}, \dots, \bar{1}\}$. Note that factorization (9) may be non-unique. What is unique is the cycle structure of the permutation on $\{1, \dots, t\}$ defined by $\tau = T \pi_e^{-1} T \pi_o$, where $T = (1\bar{1}) \cdots (t\bar{t})$ is used to “cast” the permutation π_e into a permutation acting on $\{1, \dots, t\}$.

It turns out that the class coefficients $V_N^{\text{O}}(\pi)$ depend only on the cycle type of the permutation τ defined above. They satisfy the recursion

$$(10) \quad (N + c_1) V_N^{\text{O}}(c_1, \dots, c_k) + \sum_{p+q=c_1} V_N^{\text{O}}(p, q, c_2, \dots, c_k) + 2 \sum_{j=2}^k c_j V_N^{\text{O}}(c_1 + c_j, \dots, \hat{c}_j, \dots, c_k) \\ = \delta_{c_1,1} V_N^{\text{O}}(c_2, \dots, c_k),$$

with the initial condition $V_N^{\text{O}}(\emptyset) = 1$.

In Lemma 4.13 in Section 4.2 we will give a simpler prescription for identifying the partition c_1, \dots, c_k which corresponds to a given π , bypassing the representation of π as the product in (9).

There are also expansions of $V_N^{\text{U}}(\pi)$ in inverse powers of N with coefficients expressed in terms of the number of factorizations of π of various types: primitive factorizations [37], inequivalent factorization [5], and general factorizations [20]. It is the primitive factorizations, discussed by Matsumoto and Novak [37], that will be particularly important to us. We will give an alternative proof of their result in Section 5.3 and will extend it to the COE case in Section 6.3.

²Thus, despite the word “orthogonal” in the name, it is not the orthogonal group $O(N)$. Rather, it can be identified with $U(N)/O(N)$.

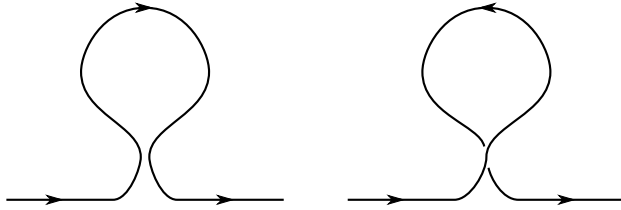


FIGURE 1. A schematic depiction of a pair of trajectories that provide the first off-diagonal contribution. This pair requires TRS, since the loop is traversed by the trajectories in opposite directions.

3. SEMICLASSICAL APPROXIMATION

In this section we review the physical approximations involved in evaluating correlations of the type

$$(11) \quad C_E(\mathbf{a}, \mathbf{b}) = \langle Z_{a_1 a_{\bar{1}}} \cdots Z_{a_s a_{\bar{s}}} Z_{b_1 b_{\bar{1}}}^* \cdots Z_{b_t b_{\bar{t}}}^* \rangle_E.$$

First one employs the semiclassical approximation [45, 60, 61] from equation (2), leading to the expression

$$(12) \quad C_E(\mathbf{a}, \mathbf{b}) = \left\langle \frac{1}{(N\tau_d)^{(s+t)/2}} \sum_{\substack{\gamma_j(a_j \rightarrow a_{\bar{j}}) \\ \gamma'_k(b_k \rightarrow b_{\bar{k}})}} \prod_{j=1}^s A_{\gamma_j} e^{\frac{i}{\hbar} S_{\gamma_j}(E)} \prod_{k=1}^t A_{\gamma'_k}^* e^{-\frac{i}{\hbar} S_{\gamma'_k}(E)} \right\rangle,$$

here $N\tau_d$ is equal to the Heisenberg time.

In the second step, which we will call the “coinciding pathways approximation”, it is argued that since \hbar is very small, the energy average is a sum of oscillatory integrals, so we first look for sets of trajectories that can have a small phase

$$\sum_j S_{\gamma_j}(E) - \sum_k S_{\gamma'_k}(E) \lesssim \hbar.$$

and contribute consistently in the semiclassical limit [65, 66, 71, 72]. For each configuration of trajectories considered in the coinciding pathway approximation, in a final step the contribution is evaluated using further semiclassical approximations involving integrals over the full range of phases.

For each configuration considered, the union of paths of γ_j in the phase space must be almost identical to the union of paths γ'_k . At this point, TRS starts to play a role: if it is broken then the paths of γ'_k must be traversed in the same direction, while in the presence of TRS the direction of traversal becomes irrelevant.

Let us consider the case $s = t = 1$ for simplicity. The easiest way to achieve a small action difference is to let $\gamma = \gamma'$. This is known as the “diagonal approximation”, pioneered for closed systems by Berry [11] using the sum rule of Hannay and Ozorio de Almeida [23], and for open systems that we consider here by Blümel and Smilansky [12]. However, it was observed in [1] that the diagonal approximation in some cases fails to predict even the leading order contribution correctly.

From analogy to disordered systems it was believed that the next off-diagonal correction would come from trajectories γ that nearly intersect themselves, thus having a loop. The partner trajectory γ' would run along γ until the self-intersection, then traverse the loop in the

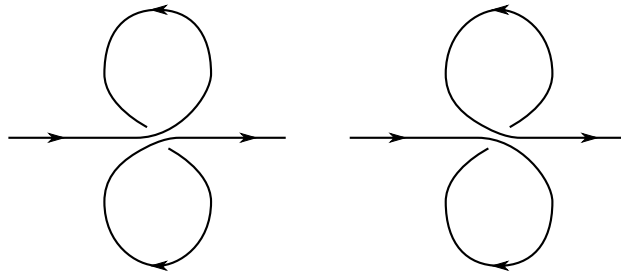


FIGURE 2. A simple pair of trajectories that do not require TRS: both loops are traversed by both trajectories in the same direction, but in a different order.

direction *opposite* to γ , and in the final part it would run along γ again. This configuration requires TRS and is schematically depicted in Fig. 1. These general ideas were given analytical form in a breakthrough work by Richter and Sieber [61] (see also [65, 66]), who calculated the correction from the diagrams shown in Fig. 1. This correction was evaluated by expressing the action difference, or phase, in terms of the angle of intersection of γ' weighted by its ergodic average of occurrence and approximated by a stationary phase integral. This development paved the way for calculating higher order corrections and higher order moments. For example, one of the simplest configurations with broken TRS is presented in Fig. 2. Before we proceed, however, it is important to mention that the trajectory γ can (and typically does) have more than one “near intersection”. The diagram of Fig. 1 is meant to represent the unique near-intersection at which the trajectories γ and γ' go in different directions.

The general idea is to split the set of paths into regions of two types: “links” (or “stretches”) that are traversed by exactly one γ_j and exactly one γ'_k and “encounters” where multiple stretches meet and the trajectories γ interconnect differently from the trajectories γ' . Using additional assumptions that all stretches are long and the sum over all possible paths a stretch can take (between two given endpoints) is well approximated by the ergodic average, Müller, Heusler, Braun and Haake [47] formulated rules for evaluating the contribution of a given topological arrangement of trajectories. This is the third major approximation involved in the Essen ansatz.

Definition 3.1. The total contribution of all pairs $\{\gamma_j\}$ and $\{\gamma'_k\}$ with a given topological arrangement of links and encounters is given by a product where

- every link provides a factor $1/N$,
- every encounter of $2l$ stretches (an l -encounter) gives a factor of $-N$,
- encounters that happen in the lead do not count (give a factor of 1).

With these approximations the problem of evaluating any transport statistic is reduced to the (hard) problem of counting all distinct topological arrangements of links and encounters, so-called “diagrams”, with their respective weights calculated according to the rules above.

The rules of Definition 3.1 ensure that the contribution to a given correlator $C_E(\mathbf{a}, \mathbf{b})$ at a given order of $1/N$ comes from a finite number of topological arrangements of trajectories. To prove Theorem 1.1 we will show that the sum over the arrangements reproduces the RMT result at *every* order of $1/N$.

4. RESTRICTIONS ON MATRIX COEFFICIENTS

Within the coinciding pathways approximation, links of the trajectories $\{\gamma_j\}$ should be in a one-to-one correspondence to links of the trajectories $\{\gamma'_k\}$. For the links starting or ending in channels in the lead, this implies restriction on which correlators from (11) can be non-zero. Here we describe these restrictions, first for the systems with broken TRS (the unitary case) as it is simpler and then for systems with TRS (the orthogonal case).

4.1. The unitary case. For the unitary case with broken TRS, assume we have a suitable configuration of trajectories γ and γ' , contributing to $C_E(\mathbf{a}, \mathbf{b})$. We start from channel a_1 and follow the trajectory γ_1 . The final stretch of γ_1 leads to the channel $a_{\bar{1}}$. With the coinciding pathways approximation, the same stretch is traversed by a γ' trajectory, which we denote by $\gamma'_{\pi(1)}$. The trajectory $\gamma'_{\pi(1)}$, by definition, goes between channels $b_{\pi(1)}$ and $b_{\overline{\pi(1)}}$. The final stretch of γ_1 must also be final for $\gamma'_{\pi(1)}$ (since it is leading to a channel and not an encounter and since the trajectories must run in the same direction). We immediately conclude that

$$(13) \quad a_{\bar{1}} = b_{\overline{\pi(1)}}.$$

We follow the trajectory $\gamma'_{\pi(1)}$ backwards, until we are on its first stretch, about to hit channel number $b_{\pi(1)}$. The partner of $\gamma'_{\pi(1)}$ on this stretch is a γ trajectory, which we will denote $\gamma_{\tau(1)}$. We can now conclude that

$$(14) \quad a_{\tau(1)} = b_{\pi(1)}.$$

We can now follow trajectory γ_2 , finding the value of $\pi(2)$ and $\tau(2)$ etcetera. It is clear that the thus defined functions π and τ are permutations. Since the number of end-points of the trajectories γ needs to be the same as the number of end-points of the trajectories γ' , we immediately get $s = t$ in Eq. (11). Henceforth we denote this common value by n .

Further, the permutation π imposes n restrictions on the sets \mathbf{a} and \mathbf{b} , namely,

$$a_{\bar{j}} = b_{\overline{\pi(j)}}, \quad j = 1 \dots n.$$

Letting $\sigma = \pi\tau^{-1}$ we can transform identities similar to (14) into

$$a_j = b_{\sigma(j)}, \quad j = 1 \dots n.$$

The permutation τ defined above and calculated from σ and π as $\tau = \sigma^{-1}\pi$ will be called the “target permutation”.

We can summarize our discussion as a lemma.

Lemma 4.1. *Let $\mathbf{a} \in \mathbb{N}^s$, $\mathbf{b} \in \mathbb{N}^t$. Within the “coinciding pathways approximation”, $C_E^U(\mathbf{a}, \mathbf{b})$ is zero unless $s = t$ and there exist permutations $\pi, \sigma \in S_t$ such that*

$$(15) \quad a_j = b_{\sigma(j)} \quad \text{and} \quad a_{\bar{j}} = b_{\overline{\pi(j)}}, \quad j = 1 \dots t.$$

Moreover, if two pairs, (π_1, σ_1) and (π_2, σ_2) , both fulfill (15) and have the same target permutation $\tau = \sigma_1^{-1}\pi_1 = \sigma_2^{-1}\pi_2$, then their contributions to $C_E^U(\mathbf{a}, \mathbf{b})$ are identical. In other words,

$$(16) \quad C_E^U(\mathbf{a}, \mathbf{b}) = \delta_{t,s} \sum_{\sigma, \pi \in S_t} \Delta^U(\sigma^{-1}\pi) \prod_{j=1}^t \delta(a_j - b_{\sigma(j)}) \delta\left(a_{\bar{j}} - b_{\overline{\pi(j)}}\right),$$

where $\Delta^U(\sigma^{-1}\pi)$ is the total contribution of trajectories γ and γ' whose ends satisfy (15).

Remark 4.2. The permutations σ and π have the same role as those appearing on the right-hand side of equation (6).

Proof. What remains to be proved in Lemma 4.1 is that the contributions of (π_1, σ_1) and (π_2, σ_2) are identical. We will exhibit a one-to-one correspondence between the set of trajectories with ends satisfying

$$(17) \quad a_j = b_{\sigma_1(j)} \quad \text{and} \quad a_{\bar{j}} = b_{\overline{\pi_1(j)}}, \quad j = 1 \dots n$$

and trajectories with ends satisfying

$$(18) \quad a_j = b_{\sigma_2(j)} \quad \text{and} \quad a_{\bar{j}} = b_{\overline{\pi_2(j)}}, \quad j = 1 \dots n.$$

To do so we simply relabel the trajectories γ' , so that the trajectory γ'_j becomes the trajectory $\tilde{\gamma}'_{\pi_2\pi_1^{-1}(j)}$. Then the second identity in (17) becomes

$$a_{\bar{j}} = b_{\overline{\pi_2\pi_1^{-1}\pi_1(j)}} = b_{\overline{\pi_2(j)}},$$

and the first one

$$a_j = b_{\pi_2\pi_1^{-1}\sigma_1(j)} = b_{\pi_2\pi_2^{-1}\sigma_2(j)} = b_{\sigma_2(j)},$$

where the equality of the target permutations was used. \square

Example 4.3. Consider the correlator

$$\langle Z_{1,2}Z_{2,1}^* \rangle_E, \quad \text{i.e.} \quad a_1 = 1, \quad a_{\bar{1}} = 2, \quad b_1 = 2, \quad b_{\bar{1}} = 1.$$

For a system with broken time reversal symmetry this correlator is zero. Indeed, there are no permutations σ and π (on 1 element) that can satisfy equations (15).

Example 4.4. Consider the correlator

$$\langle Z_{1,2}Z_{3,4}Z_{5,6}Z_{3,6}^*Z_{5,4}^*Z_{1,2}^* \rangle_E.$$

The trajectories run

$$\begin{array}{lll} \gamma_1 : 1 \rightarrow 2, & \gamma_2 : 3 \rightarrow 4, & \gamma_3 : 5 \rightarrow 6, \\ \gamma'_1 : 3 \rightarrow 6, & \gamma'_2 : 5 \rightarrow 4, & \gamma'_3 : 1 \rightarrow 2, \end{array}$$

and the variables a and b have values

$$\begin{array}{llllll} a_1 = 1, & a_{\bar{1}} = 2, & a_2 = 3, & a_{\bar{2}} = 4, & a_3 = 5, & a_{\bar{3}} = 6, \\ b_1 = 3, & b_{\bar{1}} = 6, & b_2 = 5, & b_{\bar{2}} = 4, & b_3 = 1, & b_{\bar{3}} = 2. \end{array}$$

Two examples of trajectory configurations contributing to the correlator above are given in Fig. 3. Note that the start and end of each trajectory (unfilled circles) are labelled by the index of the corresponding variable a_j or $a_{\bar{j}}$ and not by its value.

From equation (15) it is clear that the only choice for σ and τ is (in the two-line notation)

$$\sigma = \begin{pmatrix} 1 & 2 & 3 \\ 3 & 1 & 2 \end{pmatrix}, \quad \pi = \begin{pmatrix} 1 & 2 & 3 \\ 3 & 2 & 1 \end{pmatrix}.$$

Therefore, the target permutation is $\tau = (1)(23)$ (in the cycle notation). The target permutation can be read off the diagram (see Fig. 3) by starting at j , then following the γ trajectory until its end, then following the γ' trajectory in reverse to its start. The label there is the image of j under the action of τ .

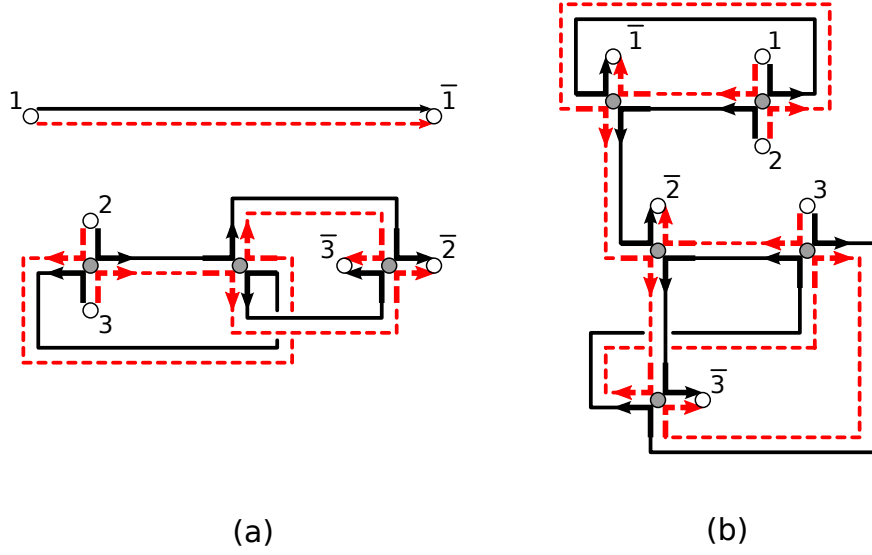


FIGURE 3. Two examples of configurations of trajectories that contribute to the correlator in Example 4.4. The endpoints of trajectories are labelled by the indices of the variables a_1, \dots, a_3 and $a_{\bar{1}}, \dots, a_{\bar{3}}$. The trajectories γ_j are drawn in black solid lines; they go from j to \bar{j} . The trajectories γ'_j are drawn in red dashed line and go from $\tau(j)$ to \bar{j} .

Example 4.5. For the correlator

$$\langle Z_{1,2} Z_{3,2} Z_{1,2}^* Z_{3,2}^* \rangle_E$$

there are two choices of the pair (σ, π) . The mapping σ between the first indices is the identity permutation id , while the mapping between the second indices can either be id or (12) . Therefore the target permutation τ is

$$\tau = id \quad \text{or} \quad \tau = (12).$$

Remark 4.6. Consider the correlator of the type

$$\langle Z_{i_1, o_1} Z_{i_2, o_2} \cdots Z_{i_n, o_n} Z_{i_2, o_1}^* Z_{i_3, o_2}^* \cdots Z_{i_1, o_n}^* \rangle,$$

which arise in evaluation of moments (4). Irrespective of the choices of the values for the indices i_1, \dots, o_n , one can always let

$$\sigma = (n \dots 21), \quad \pi = id.$$

leading to τ being the grand cycle, $\tau = (12 \dots n)$. In previous papers, starting with [4], the diagrams realizing this choice of τ were considered as the base contribution. Correcting factors were used to take care of other target permutations, arising, for example, when $i_j = i_k$ for some j and k . It was argued that other target permutations corresponded to encounters happening in a lead (which essentially removes the encounter from the diagram, see the rules of the Essen ansatz). An encounter in the base diagram that *could* be moved into the lead can be seen as “untying” the encounter. We consider this interpretation in detail in the second half of this work [9] since it provides an easier way to obtain answers for the moment generating functions.

For the proof of our main theorem, however, it is more convenient to have each diagram representing one target permutation and to sum over the target permutation, as is already done on the RMT side. The work by Novaes [54, 55] adopts a similar strategy.

4.2. The orthogonal case. In the presence of TRS there are more possibilities to match parts of the trajectories γ to γ' , since now the “head” can be matched with the “tail”.

More precisely, the channel a_1 lies at the start of the trajectory γ_1 but must also lie on a trajectory γ'_j . Therefore a_1 must coincide either with b_j or $b_{\bar{j}}$. In other words,

$$a_1 = b_{\varpi(1)},$$

where $\varpi(1) \in \{1, \dots, t, \bar{t}, \dots, \bar{1}\}$. Similarly for all other channels a_j there is a matching channel $b_{\varpi(j)}$, where j can be $1, \dots, t$ or $\bar{t}, \dots, \bar{1}$. This defines the permutation ϖ on $2t$ symbols $Z_t = \{1, \dots, t, \bar{t}, \dots, \bar{1}\}$. Thus the only restriction on the indices a_j and b_j is that they are equal as multi-sets (i.e. contain the same elements the same number of times).

Notation 4.7. In the description of orthogonal trajectories, we adopt the convention that j or k refers to the variable label that does not have the bar (correspondingly, \bar{j} is a label that does have the bar), while z denotes a label either with or without the bar.

To understand the analogue of the *target permutation* in the orthogonal case, we take another look at the unitary case. The target permutation was $\tau = \sigma^{-1}\pi$. However, it could be argued that π and σ act on different spaces: σ acts on the elements $\{1, \dots, t\}$ and π acts on $\{\bar{1}, \dots, \bar{t}\}$. To multiply the permutations we need to map them onto the same space, for example using the mapping $T : j \mapsto \bar{j}$. Then the “correct” expression for the target permutation is $\tau = \sigma^{-1}T^{-1}\pi T$.

This correction, somewhat superfluous in the unitary case, becomes a necessity in the orthogonal case. The meaning of the mapping T is “propagation along the trajectory” γ or γ' . We define it as a permutation on Z_t :

$$T = (1\bar{1}) \cdots (t\bar{t}).$$

In particular, T is an involution, i.e. $T^{-1} = T$. Moreover, in the orthogonal case, the permutation ϖ plays the role of π and σ *combined*. We thus define the target permutation τ by

$$(19) \quad \tau = \varpi^{-1}T^{-1}\varpi T.$$

It acts on the ends of trajectories γ in the following fashion: take an end, propagate along γ to the other end, find the corresponding end of a trajectory γ' , propagate to its other end. This is the corresponding end of the next γ -trajectory.

Example 4.8. Consider the correlator $\langle Z_{12}Z_{34}Z_{56}Z_{54}^*Z_{31}^*Z_{62}^* \rangle$. The permutation ϖ (in two-row notation) is

$$\varpi = \begin{pmatrix} 1 & \bar{1} & 2 & \bar{2} & 3 & \bar{3} \\ \bar{2} & \bar{3} & 2 & \bar{1} & 1 & 3 \end{pmatrix}.$$

Then the target permutation is $\tau = (1\bar{3}\bar{2})(23\bar{1})$. Two examples of trajectory configurations contributing to the correlator above are given in Fig. 4

Example 4.9. Consider the correlator $\langle Z_{12}Z_{31}Z_{23}^*Z_{11}^* \rangle$. There are two possibilities for the permutation φ , namely

$$\varpi = \begin{pmatrix} 1 & \bar{1} & 2 & \bar{2} \\ 2 & 1 & \bar{1} & \bar{2} \end{pmatrix} \quad \text{and} \quad \varpi = \begin{pmatrix} 1 & \bar{1} & 2 & \bar{2} \\ \bar{2} & 1 & \bar{1} & 2 \end{pmatrix}.$$

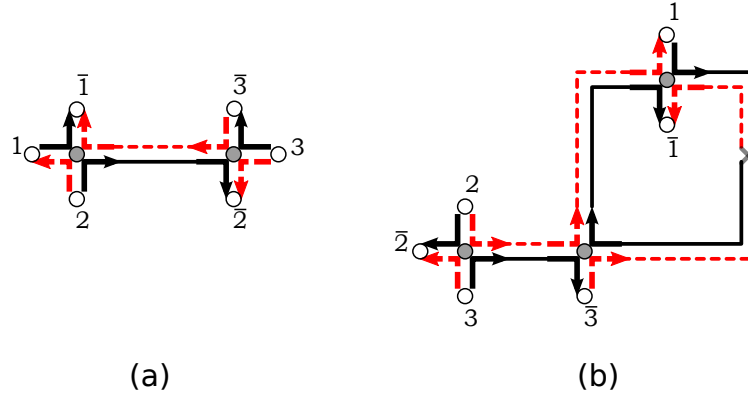


FIGURE 4. Two examples of trajectory configurations contributing to the correlator of Example 4.8. In the second diagram, to draw the trajectories on the plane we had to allow them to cross.

Both of these correspond to the same target permutation $\tau = (12)(\bar{2}\bar{1})$.

Note the “palindromic” symmetry of the results of Examples 4.8 and 4.9. This observation is made precise in the following Lemma.

Lemma 4.10. *The orthogonal target permutation has the following properties:*

- (1) if $\tau(x) = y$ then $\tau(\bar{y}) = \bar{x}$,
- (2) $\tau(x) \neq \bar{x}$.

Therefore the cycles on τ come in symmetric pairs: for every cycle $(z_1 z_2 z_3 \dots)$ there is the distinct partner cycle $(\dots \bar{z}_3 \bar{z}_2 \bar{z}_1)$.

Proof. Denote $\varpi(\bar{x}) =: z$. Then we have $y = \tau(x) = \varpi^{-1}T^{-1}\varpi(\bar{x}) = \varpi^{-1}(\bar{z})$. Therefore $\varpi(y) = \bar{z}$.

Now we can calculate $\tau(\bar{y}) = \varpi^{-1}T^{-1}\varpi(y) = \varpi^{-1}(z) = \bar{x}$.

For the second property, we assume the contrary: $\tau(x) = \bar{x}$. Then $\varpi^{-1}T^{-1}\varpi(\bar{x}) = \bar{x}$ or the contradiction

$$\varpi(\bar{x}) = \overline{\varpi(\bar{x})}.$$

The conclusion now follows. Indeed the first property implies that for every cycle $(z_1 z_2 z_3 \dots)$ there is the cycle $(\dots \bar{z}_3 \bar{z}_2 \bar{z}_1)$. The fact that these are not the same cycle follows from the second property. \square

Remark 4.11. Property 1 of Lemma 4.10 can be written as $\tau(T\tau(x)) = \bar{x}$ or, equivalently, $T\tau T\tau = id$. In other words, $T\tau$ is an involution. Property 2 is equivalent to $T\tau(x) \neq x$. Therefore, Lemma 4.10 can be reformulated as saying that $T\tau$ consists only of cycles of length 2.

Remark 4.12. An equivalent way to express the symmetry of τ is via the identity $\tau(x) = \overline{\tau^{-1}(\bar{x})}$. This is similar to the definition of the *hyperoctahedral group* that is the subgroup of S_{2t} with elements satisfying $\chi(x) = \overline{\chi(\bar{x})}$. However, our target permutations are different, since they do not form a group.

There is a close connection between the target permutation τ and the cycle structure appearing as the true parameters of the class coefficients V_N^{O} , see (7).

Lemma 4.13. *Let the permutation ϖ be represented as the product $T'\pi_o\pi_eT''$, where T' and T'' are some involutions that contain only cycles of the form $(j)(\bar{j})$ or $(j\bar{j})$, π_o is a permutation on the set $\{1, \dots, t\}$ and π_e is a permutation on the set $\{\bar{t}, \dots, \bar{1}\}$, see Section 2.*

Then the cycle type of $\tau = \varpi^{-1}T^{-1}\varpi T$ is twice that of the permutation $T\pi_e^{-1}T\pi_o$. Consequently, the latter cycle type does not depend on the choice of the representation.

Proof. Substituting the representation $\varpi = T'\pi_o\pi_eT''$ into the definition of τ and noting that the involutions T' , T'' and T commute, we get

$$\tau = T (T''\pi_e^{-1}\pi_o^{-1}T') T (T'\pi_o\pi_eT'') = T'' (T\pi_e^{-1}T) (T\pi_o^{-1}T) \pi_o\pi_e T'' \sim (T\pi_e^{-1}T\pi_o) (T\pi_o^{-1}T\pi_e),$$

where \sim denotes conjugate permutations. Obviously, the two parts of the last expression act on disjoint sets $\{1, \dots, t\}$ and $\{\bar{t}, \dots, \bar{1}\}$ and have the same cycle type, which explains the doubling. \square

A result analogous to Lemma 4.1 summarizes the discussion of this section.

Lemma 4.14. *Let $\mathbf{a} \in \mathbb{N}^s$, $\mathbf{b} \in \mathbb{N}^t$. Within the “coinciding pathways approximation”, $C_E^{\text{O}}(\mathbf{a}, \mathbf{b})$ is zero unless $s = t$ and there exists a permutation ϖ on $Z_t = \{1, \dots, t, \bar{t}, \dots, \bar{1}\}$ such that*

$$(20) \quad a_z = b_{\varpi(z)}, \quad z \in Z_t.$$

Moreover, if two permutations, ϖ_1 and ϖ_2 , both fulfill (20) and have the same target permutation $\tau = \varpi_1^{-1}T^{-1}\varpi_1T = \varpi_2^{-1}T^{-1}\varpi_2T$, then their contributions to $C_E^{\text{O}}(\mathbf{a}, \mathbf{b})$ are identical. In other words,

$$(21) \quad C_E^{\text{O}}(\mathbf{a}, \mathbf{b}) = \delta_{t,s} \sum_{\varpi \in S_{2t}} \Delta^{\text{O}}(\tau) \prod_{z \in Z_t} \delta(a_z - b_{\varpi(z)}),$$

where $\Delta^{\text{O}}(\tau)$ is the total contribution of trajectories γ and γ' whose ends satisfy (20).

Proof. As before, the only part we need to prove is that the contributions of trajectories satisfying (20) with ϖ_1 and ϖ_2 are identical if the corresponding target permutations coincide. Starting with a set of trajectories described by ϖ_1 we will relabel them so that they will be described by ϖ_2 . We will only relabel the partner trajectories γ' . Note that direction-reversal is allowed.

The relabelling permutation we will denote by ρ . It acts on the ends of the trajectories, namely if the original trajectory γ'_j run from b_j to $b_{\bar{j}}$, the new one $\tilde{\gamma}'_j$ runs from $\tilde{b}_j = b_{\rho(j)}$ to $\tilde{b}_{\bar{j}} = b_{\rho(\bar{j})}$.

We want to have $a_z = \tilde{b}_{\varpi_2(z)}$. On one hand we have $a_z = b_{\varpi_1(z)}$ (since the original trajectories agreed with ϖ_1). On the other, we have $\tilde{b}_{\varpi_2(z)} = b_{\rho(\varpi_2(z))}$. Therefore, ρ needs to satisfy $\rho\varpi_2 = \varpi_1$, or

$$\rho = \varpi_1\varpi_2^{-1}.$$

We now verify that ρ is a valid relabelling. Namely, if it maps the trajectory end j to the trajectory end k (or \bar{k}), then it must map the other end \bar{j} to \bar{k} (correspondingly, k). Putting it formally, ρ must satisfy $\rho T = T\rho$. By the definition of the target permutation (and since T is an involution), we have $\varpi_2^{-1}T = \tau T\varpi_2^{-1}$. Therefore,

$$\rho T = \varpi_1\varpi_2^{-1}T = \varpi_1\tau T\varpi_2^{-1} = \varpi_1(\varpi_1^{-1}T\varpi_1)\varpi_2^{-1} = T\varpi_1\varpi_2^{-1} = T\rho,$$

as desired. □

5. SUMMATION OVER THE UNITARY DIAGRAMS

Diagrams are schematic depictions of sets of trajectories, describing which parts of trajectories $\{\gamma_j\}$ follow which parts of trajectories $\{\gamma'_j\}$ by using a graph whose edges correspond to stretches of γ and vertices correspond to encounters (see section 3).

In this section we describe how the diagrams can be encoded mathematically, operations acting within the set of diagrams and the cancellations resulting when we evaluate the contributions Δ^U as a sum over all possible diagrams. We will consider here the case of broken TRS (“unitary” diagrams) before treating TRS in section 6.

5.1. Diagrams as ribbon graphs. The drawings in Fig. 3 hint that the natural mathematical description of the topology of a set of contributing trajectories is a *ribbon graph*, also known as a *fat graph* or a *map*. In combinatorics, a *map* is a graph which is drawn on a surface in such a way that (a) the edges do not intersect and (b) cutting the surface along the edges one obtains disjoint connected sets (“countries”), each homeomorphic to an open disk. The act of drawing a graph on surface fixes a cyclic ordering of the edges incident to each vertex. For an accessible introduction to combinatorial maps and their application to RMT (which is only one of their numerous applications) we refer the reader to [81]. Further information can be found in [26, 73], among other sources. Note that in the present article we only use the term “map” in the combinatorial sense.

Lacking a surface of sufficiently high genus, maps can be drawn on a sheet of paper (though the edges might need to intersect). It is convenient to fatten the edges of such graphs to make them *ribbons*, with two sides, and represent the maps as *ribbon graphs*. At vertices, which are also fattened, the side of one edge is connected to a side of another, which corresponds to the cyclic ordering mentioned above. Following the sides until we return to the starting spot we trace out *boundary walks* of the map.

In semiclassical diagrams, each trajectory stretch corresponds to a fattened edge of the graph. The trajectory γ runs along one side of the edge and γ' runs (in the same direction) along the other side. The vertices of degree 1, henceforth called *leaves*, correspond to trajectories either starting from or exiting into a channel. They are labelled by the symbols $1, \dots, t$ and $\bar{1}, \dots, \bar{t}$, which are understood to correspond to the indices of the variables \mathbf{a} and \mathbf{b} in the correlator $C_E(\mathbf{a}, \mathbf{b})$, equation (11). All other vertices correspond to encounters which we will refer to as *internal* vertices. At a vertex the trajectory can be followed by continuing along the side of the edge onto the side of the vertex and then on to the corresponding side of the next edge.

The ribbon graphs used in the present article are not significantly different from the more traditional way the semiclassical diagrams are depicted in the physics literature (see, e.g. [10, 47, 49, 69]). In the “physics” diagrams, the trajectories are shown as smooth with the reconnections (which distinguish trajectories γ from trajectories γ') happening in the small encounter regions, see Fig. 5. Within the encounter region trajectories are drawn as intersecting. This has the unfortunate effect of confining a lot of information to a small part of the drawing.

We “untwist” the encounter regions as shown in Figs. 6(a) and (b), making sure the trajectories do not intersect at encounters (vertices). Some intersections or twists might still be necessary, due to high genus or non-orientability of the graph, but these are shifted away from vertices to avoid overloading them with detail. This way of drawing allows the interpretation of

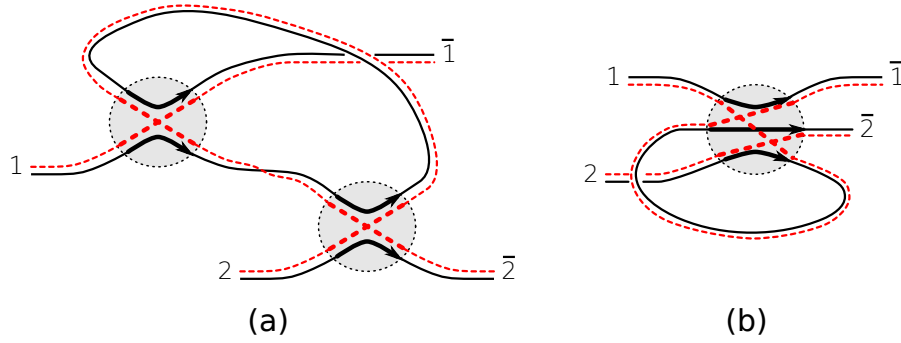


FIGURE 5. Two examples of semiclassical diagrams as drawn in the physics literature. These examples correspond to diagrams (d) and (e) of Fig. 4 in [47]

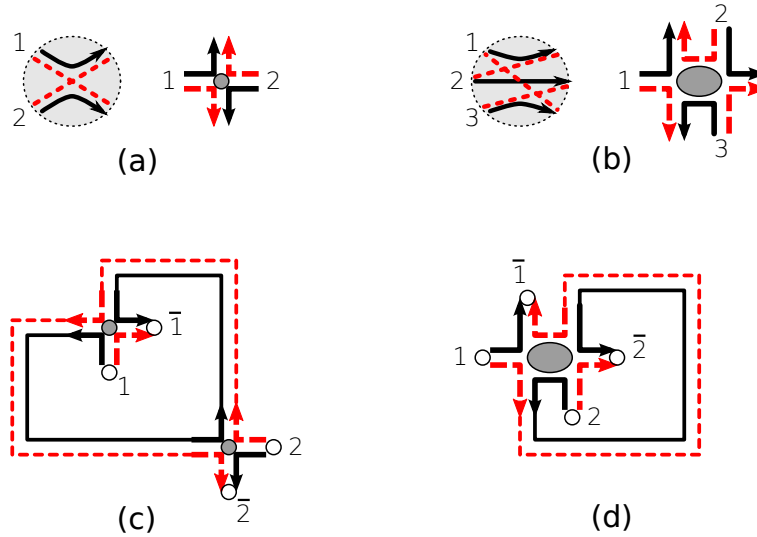


FIGURE 6. Untwisting the encounters into the vertices of the ribbon graph, (a) and (b). The ribbon graphs (c) and (d) correspond to the diagrams of Fig. 5. To read off the trajectories, we start at the open end labelled 1 and follow the left side for γ or the right side for γ' . The leaves (vertices of degree 1) of the graph are shown as empty circles; the internal vertices are represented by the filled ellipses. Edges going to leaves are normally drawn short to save space. Other edges often have rectangular corners; the corners carry no particular meaning and were employed only due to the lack of artistic skill.

the trajectories as parts of the boundary of the resulting ribbon graphs and opens the area up to a variety of existing combinatorial methods.

We formalize the above paragraphs as a definition.

Definition 5.1. The *unitary diagram* with the target permutation τ is a map satisfying the following:

- (1) There are t vertices of degree 1 (henceforth *leaves*) labelled with symbols $1, \dots, t$ and t leaves labelled with symbols $\bar{1}, \dots, \bar{t}$.

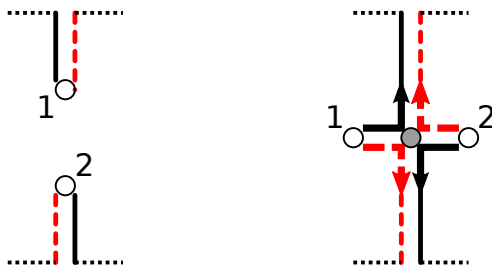


FIGURE 7. The operation of tying two leaves together. By dotted lines we represent the rest of the graph.

- (2) All other vertices have even degree greater than 2.
- (3) A portion of the boundary running from one leaf to the next is called a *boundary segment*. Each leaf z is incident to two boundary segments, one of which is a segment running between leaves j and \bar{j} and the other between leaves $\tau(k)$ to \bar{k} (where either $z = j = \tau(k)$ or $z = \bar{j} = \bar{k}$). The segments are given direction $j \rightarrow \bar{j}$ and $\tau(k) \rightarrow \bar{k}$ and marked by solid and dashed lines correspondingly. The following conditions are satisfied:
 - (a) each part of the boundary is marked exactly once,
 - (b) each edge is marked solid on one side and dashed on the other, both running in the same direction.

We will now discuss some properties of the diagrams that follow from the basic definition above.

The boundary segments marked solid correspond to the γ -trajectories and dashed correspond to γ' -trajectories. The boundary walks of the map can be read by alternately following γ and γ' (in reverse) trajectories. Then each edge is traversed in opposite directions on the two sides, which means the graph is orientable [73, Chap. X]. The labels of the leaves are arranged in a special way: a trajectory γ starts at a vertex j and ends at \bar{j} . The trajectory γ' that immediately follows it, starts (when read in reverse) at \bar{j} and ends at $\tau(j)$, where τ is the target permutation of the diagram in question, see the discussion of Section 4.1. To summarize,

Lemma 5.2. *A unitary diagram satisfies the following properties:*

- (1) *The map is orientable.*
- (2) *Each boundary walk passes through a non-zero even number of leaves. Their labels form the sequence of the form*

$$j, \bar{j}, \tau(j), \overline{\tau(j)}, \tau^2(j), \dots, \overline{\tau^f(j)},$$

where τ is the target permutation of the diagram and $\tau^{f+1}(j) = j$. This establishes a one-to-one correspondence between the boundary walks and the cycles of τ .

5.2. Operations on diagrams. We now define some operation on diagrams which will later allow us to find cancellations of their contributions evaluated according to Definition 3.1.

The first operation is *tying* together two leaves. Given two leaves j and k (with no bars) we form a new vertex of degree 4 as shown in Fig. 7. Note that the trajectory γ connected to the vertex j is still connected to j after tying, whereas the γ' trajectory becomes connected to k . Tying two leaves together creates an internal vertex and two edges.

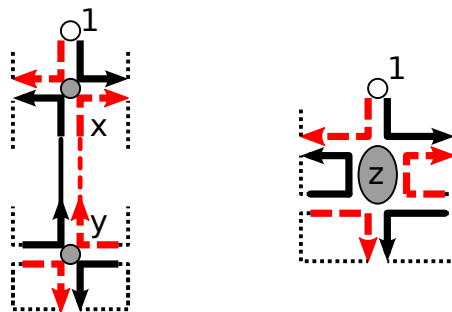


FIGURE 8. The operation of contracting an edge. By dotted lines we represent the rest of the graph.

The reversal of this operation is *untying*. It can only be performed if there are two leaves (without bars) attached on the opposite sides of the vertex of degree 4 that is to be untied.

Lemma 5.3. *Consider a diagram with the target permutation τ . If we tie the leaves j and k together, the target permutation of the modified diagram is $(j k)\tau$. Untying a 4-vertex with leaves j and k directly attached to its opposite sides also results in the target permutation $(j k)\tau$.*

Proof. The target permutation is read off a diagram by following a γ -trajectory (solid, black lines in the figures) from a leaf i to the next leaf (which must be \bar{i}) and then following the γ' -trajectory (dashed, red lines) in reverse until the next leaf which is the leaf $\tau(i)$. When the leaves j and k are tied together, the γ -trajectories are not changed, but the γ' -trajectories that originated from j and k are switched around. Thus the target permutation of the modified diagram acts as the permutation τ followed by the interchange of j and k . Hence the multiplication by $(j k)$ *on the left*.

Untying the vertex with leaves j and k is thus equivalent to multiplying by the inverse of $(j k)$, which is the same as multiplying by $(j k)$ itself. \square

This operation of tying can be generalized to the case of two leaves with bars and to the case of more than two leaves (of the same kind – either all with or all without bars). The reversal, untying, will only work on a vertex of degree $2m$ if there are m leaves of the same kind attached to it. In terms of the target permutations, the tying of several leaves without bars is equivalent to multiplying by the cycle of length m . The tying of leaves with bars is multiplication by the cycle *on the right* and untying is multiplication by the inverse cycle on the appropriate side. The precise order of the elements in the cycle has to agree with the spatial arrangement of the leaves around the cycle. However, we will not need these operations in our proofs and thus omit the precise details here. We will need these generalisations however to obtain moment generating functions as in the accompanying paper [9], so we provide full details there.

The second operation we will need is *contracting an edge*. While any edge connecting two (internal) vertices in a diagram can be contracted to produce another diagram, we will only apply this operation in the precise circumstances described below.

In order to contract an edge going between vertices x and y , see Fig. 8, we require that the vertex x has degree 4 and that the edge attached to x *opposite* the edge (x, y) is coming directly from the leaf number 1. The vertex y has no restrictions, in particular it can be of any even degree.

The operation of contracting an edge leads to the diagram with a larger vertex, shown on the right of Fig. 8. We can reverse the operation if we have a vertex of an even degree larger than 4 and an edge connecting the vertex to leaf 1. As the figure suggests, the new vertex inherits the edge to 1 and the two neighbouring edges. This operation is called *splitting the vertex*. The following lemma is obvious.

Lemma 5.4. *The operations of contracting an edge or splitting the vertex do not change the target permutation.*

In some cases considered later the diagram will have no leaf with number 1. In such a case the leaf with the smallest number will play the role of leaf 1.

5.3. Cancellations among unitary diagrams. The result of Lemma 4.1 states that the semi-classical correlator $C_E^U(\mathbf{a}, \mathbf{b})$ can be expressed as

$$C_E^U(\mathbf{a}, \mathbf{b}) = \delta_{t,s} \sum_{\sigma, \pi \in S_t} \Delta^U(\tau) \prod_{j=1}^t \delta(a_j - b_{\sigma(j)}) \delta\left(a_{\bar{j}} - b_{\pi(\bar{j})}\right),$$

where $\Delta^U(\tau)$ is the sum of contributions of diagrams with the target permutation $\tau = \sigma^{-1}\pi$. The contribution of every diagram is evaluated according to the rules in Definition 3.1. Namely, each internal vertex of a diagram gives a factor of $(-N)$ and each edge (including the ones leading to the leaves) a factor of $1/N$. Denoting by $D_{v,e}^U(\tau)$ the number of diagrams with the target permutation τ , v internal vertices and e edges, we have the following statement, which finished the proof of Theorem 1.1 in the case of broken time-reversal symmetry.

Theorem 5.5. *The total contribution of the unitary diagrams with target permutation τ is*

$$(22) \quad \Delta^U(\tau) := \sum_{v,e} D_{v,e}^U(\tau) \frac{(-1)^v}{N^{e-v}} = V_N^U(\tau).$$

Proof. The proof of the theorem has two parts. In the first part we exhibit cancellations among the diagrams. In the second part, the diagrams that survive cancellations will be shown to satisfy the same recursion as $V_N^U(\tau)$ with the same initial conditions.

The cancellation is based on the operations described in Section 5.2. We define an involution P on the set of diagrams which changes v by one but leaves $(e - v)$ invariant. This means that the two diagrams that are images of each other under P produce contributions to the sum in (22) that are equal in magnitude but opposite in sign. The sum therefore reduces to the sum over the fixed points of P . Since each diagram has many edges and vertices, the main difficulty in describing P is to uniquely specify the edge to be contracted or the vertex to be split.

The involution P is described by the following algorithm:

- (1) Find the leaf with minimal number j (without bar).
- (2) If it is attached to a vertex of degree 4 whose opposite edge ends in a leaf, *untie* the node and return to step 1. If the untying produces an edge which directly connects two leaves (k and \bar{k}), this edge is removed from consideration.
- (3) If the leaf j is attached to a node of degree 4 whose opposite edge leads to another internal vertex, *contract* the edge.
- (4) Otherwise, the leaf j is attached to a vertex of degree 6 or higher. We *split* this vertex into two by inserting a new edge.
- (5) Reverse all operations performed in step 2.

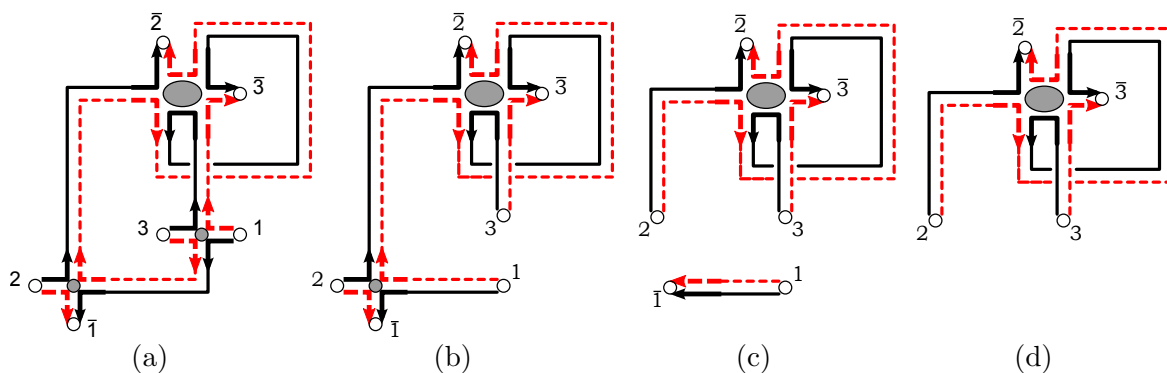


FIGURE 9. Repeatedly applying steps 1 and 2 of the cancellation algorithm. Part (a) is the original diagram. The node (13) has been untied in (b); the node (12) has been untied in (c). The edge connecting 1 and $\bar{1}$ has been removed in (d) so that 2 is the minimal leaf, but the diagram cannot be untied any further.

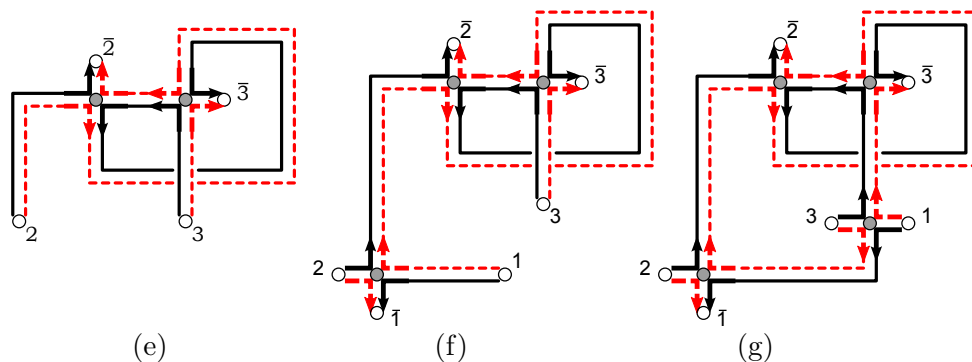


FIGURE 10. Applying steps 4 and 5 of the cancellation algorithm. Part (e) is the result of splitting the 6-vertex of Fig. 9(d) into two. Parts (f) and (g) are tying of the leaves (12) and (13) correspondingly. The diagram in part (g) is the counterpart of the original diagram in Fig. 9(a).

The algorithm is illustrated by an example in Figs. 9 and 10. The original diagram is Fig. 9(a) and the result is in Fig. 10(g). However, if we start with Fig. 10(g) and apply the algorithm, we would use step 3 instead of step 4 and arrive at Fig. 9(a).

The algorithm preserves the target permutation (see Lemma 5.4), therefore both diagrams contribute to the same sum. Note that at most one of the operations in steps 3 and 4 are performed. These operations are the inverses of each other and provide the required difference in the number v while leaving $(e - v)$ invariant. If the steps 3 or 4 are never reached, by virtue of the diagram untying completely, the corresponding contribution does not cancel and has to be counted.

Consider a diagram that unties completely (for example, the diagram in Fig. 3(a)). Recording the untyings, as suggested by Lemma 5.3, we get

$$(23) \quad (s_v r_v) \cdots (s_2 r_2) (s_1 r_1) \tau = id, \quad s_j < r_j,$$

where the identity permutation on the right corresponds to the resulting “empty” diagram. The condition in step 1 of the algorithm ensures that if $j < k$ then $s_j \leq s_k$. Given the sequence of untyings, we can reconstruct the diagram uniquely, therefore the diagrams that survive the cancellations are in one-to-one correspondence with the factorizations of τ into a product of transpositions satisfying

$$(24) \quad \tau = (s_1 r_1)(s_2 r_2) \cdots (s_v r_v), \quad s_j < r_j, \quad s_j \leq s_{j+1}.$$

These are known as *primitive factorizations*³ that are counted by *monotone single Hurwitz numbers* [22, 37]. It is known [37] that the number of such factorizations provides the coefficients in the asymptotic expansion of the class coefficients $V_N^U(\tau)$. Here we provide a basic alternative proof of this fact that will be easy to generalize to the orthogonal case.

Denote by $p_v^U(\tau)$ the number of primitive factorizations of the target permutation τ into v transpositions. We have shown that

$$(25) \quad \Delta^U(\tau) = \sum_v p_v^U(\tau) \frac{(-1)^v}{N^{e-v}},$$

where the number of edges e can be related to the other quantities as follows. First, the permutation τ is a permutation on t elements. The completely untied graph with $2t$ leaves contains t edges. Each tying increases the number of edges by 2 and the number of internal vertices by one. Since each of the v transpositions corresponds to a tying, we end up with $e = t + 2v$ edges.

The quantity $p_v^U(\tau)$ depends only on the cycle structure of τ so let c_1, \dots, c_k be the lengths of the cycles. Without loss of generality, we take $\tau = (1 2 \dots c_1) \cdots (t - c_k + 1 \dots t)$. Consider the term $(s_1 r_1)$ on the left of a primitive factorization of τ . Without this term, it is also a factorization, but of the permutation $(s_1 r_1)\tau$ and into $v - 1$ factors.

For $s_1 = 1$, we will now investigate the cycle structure of the permutation $(1 r_1)\tau$. If r_1 belongs to the first cycle of τ (i.e. the one that contains 1) it splits into two, of lengths q and r with $q + r = c_1$. Otherwise, if r_1 belongs to cycle number $j > 1$, the first cycle joins with it to form a cycle of length $c_1 + c_j$.

Finally, it can happen that $s_1 \neq 1$, but only if the element 1 does not appear in any transposition of the factorization (equivalently, the leaf 1 is attached directly to the leaf $\bar{1}$). This can happen only if 1 is in cycle of its own within the permutation τ , that is if $c_1 = 1$. In this case, the given primitive factorization is also a factorization of the permutation on $t - 1$ element with cycle lengths c_2, \dots, c_k . Altogether we have

$$(26) \quad p_v^U(c_1, \dots, c_k) = \delta_{c_1, 1} p_v^U(c_2, \dots, c_k) + \sum_{q+r=c_1} p_{v-1}^U(q, r, c_2, \dots, c_k) + \sum_{j=2}^k c_j p_{v-1}^U(c_1 + c_j, \dots, \hat{c}_j, \dots).$$

The notation \hat{c}_j again means that c_j is removed from the lengths of the cycles. We would like to substitute this recursion into (25) and we need to calculate the power of N^{-1} at which the terms of (26) would enter the sum in Δ^U . On the left, we have $e - v = (t + 2v) - v = t + v$. The first term on the right corresponds to permutations on $t - 1$ elements, hence the power is $t + v - 1$. The other two terms on the right have the same t , but a reduced number of internal

³The traditional definitions are slightly different from ours in ordering the second elements of the transpositions

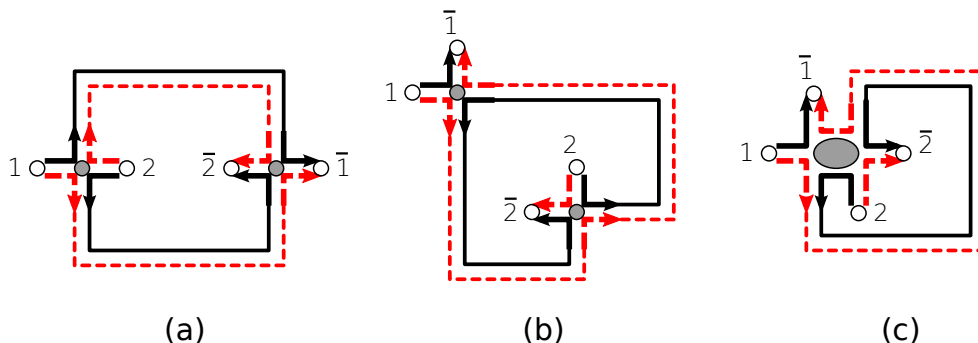


FIGURE 11. Diagrams contributing to the second term of the expansion of $V^U(id_2)$, see Example 5.6.

vertices (factors in the factorization), also resulting in $t + v - 1$. Altogether, we get (27)

$$N\Delta^U(c_1, \dots, c_k) = \delta_{c_1, 1}\Delta^U(c_2, \dots, c_k) - \sum_{q+r=c_1} \Delta^U(q, r, c_2, \dots, c_k) - \sum_{j=2}^k c_j \Delta^U(c_1 + c_j, \dots, \hat{c}_j, \dots),$$

exactly mirroring the recursion relations for V_N^U given in (8). \square

Example 5.6. Consider the contribution $\Delta^U(id_2)$, where id_2 is the identity permutation on 2 elements. According to Lemma 4.1, this contribution arises for the correlator $\langle S_{12}S_{34}S_{12}^*S_{34}^* \rangle$ or as part of many other correlators. The random matrix prediction for this is

$$V^U(id_2) = \frac{1}{N^2 - 1} = \frac{1}{N^2} + \frac{1}{N^4} + \dots$$

The first term arises from the trajectories $\gamma_1 = \gamma'_1$ and $\gamma_2 = \gamma'_2$, the corresponding diagram consisting of two disjoint edges connecting 1 to $\bar{1}$ and 2 to $\bar{2}$ correspondingly.

The diagrams contributing to the second term are depicted in Fig. 11. There are 5 diagrams altogether, with the additional two obtained from Fig. 11(b) and (c) by a shift in the leaf labeling. For example swapping the labels in Fig. 11(b) gives Fig. 5(a) and Fig. 6(c). Note that the diagrams in Fig. 11(b) and (c) are related by the involution P described in the proof of Theorem 5.5. Indeed, in the diagram in part (b) we cannot untie any vertices. We therefore go to step (3) of the algorithm and contract the edge going from the top shaded vertex to the right. The result of this edge contraction is the diagram in part (c). The diagram in part (b) has $v = 2$ and $e = 6$ and therefore contributes $(-1)^2/N^{(6-2)}$ to $\Delta^U(id_2)$. The diagram in part (c) has $v = 1$ and $e = 5$ and contributes $-1/N^{5-1}$; these contributions cancel.

The diagram in Fig. 11(a) can be untied completely and corresponds to the primitive factorization

$$id = (12)(12).$$

In fact the only primitive factorizations are of the form

$$id = (12)^{2n},$$

recreating the random matrix prediction.

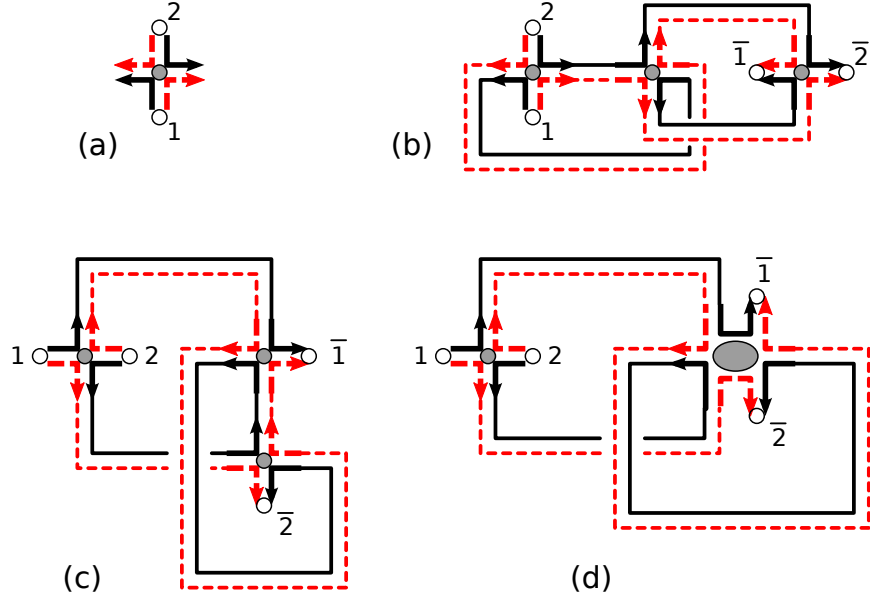


FIGURE 12. Diagrams contributing to the expansion of $V^U((12))$, see Example 5.7.

Example 5.7. Consider the contribution $\Delta^U((12))$, which is predicted by RMT to be

$$\Delta^U((12)) = -\frac{1}{N(N^2 - 1)} = -\frac{1}{N^3} - \frac{1}{N^5} - \dots$$

The first term is produced by the diagram in Fig. 12(a) with primitive factorization (12). The second term comes from the diagram in Fig. 12(b), which corresponds to the factorization

$$(12) = (12)(12)(12).$$

All other diagrams at this order (of which Figs. 12(c) and (d) are two examples) mutually cancel.

Considering the diagram in part (c) in more detail, we can untie the left shaded vertex. The leaf number 1 is now attached to the top right shaded vertex, which cannot be untied. We therefore contract the edge connected the two shaded vertices, tie leaves 1 and 2 back and arrive to the diagram in part (d).

The higher order terms in the random matrix prediction come from the unique primitive factorization

$$(12) = (12)^{2n+1}.$$

While it is possible, in principle, to list all diagrams contributing to a given moment of conductance fluctuations, a modification of the method described in the follow-up paper [9] is better suited to the task. We stress, however, that our results guarantee that the semiclassical evaluation will always agree with RMT.

6. SUMMATION OVER THE ORTHOGONAL DIAGRAMS

Building on the results for systems with broken TRS, we now turn to the case of TRS. We first develop the mathematical description of the “orthogonal” diagrams before summing their contributions.

6.1. Orthogonal diagrams as ribbon graphs. As before, in the description of orthogonal diagrams, variables j or k refer to the leaf label that does not have the bar (correspondingly, \bar{j} is a label that does have the bar), while z denotes a label either with or without the bar.

The conditions that make a valid orthogonal diagram are almost identical to the unitary case. The only significant difference is that trajectories γ and γ' do not have to run in the same direction.

Definition 6.1. The *orthogonal diagram* with the target permutation τ is a locally orientable map satisfying the following:

- (1) There are t leaves labelled with symbols $1, \dots, t$ and t leaves labelled with symbols $\bar{1}, \dots, \bar{t}$.
- (2) All other vertices have even degree greater than 2.
- (3) Each leaf is incident to two boundary segments, one of which runs between labels z_1 and \bar{z}_1 and is marked solid, and the other runs between labels $\tau(z_2)$ and \bar{z}_2 and is marked dashed. Each edge is marked solid on one side and dashed on the other.

Since τ does not preserve the two “halves” of the set $Z_t = \{1, \dots, t, \bar{t}, \dots, \bar{1}\}$, there can be boundary segments running between j and k or between \bar{j} and \bar{k} (see Fig. 4 for some examples). Thus there is no natural way to assign direction to the boundary segments. However, when we consider moment generating functions [9] we will again have a natural direction and for this reason we retain the directional arrows in the figures of orthogonal diagrams.

The consequence of dropping the direction requirement in Definition 6.1 is that we now need both orientable and (globally) non-orientable diagrams. Therefore, when drawn on a plane, some edges of the map might have twists in them: going around a graph on a closed walk can bring you back on the reverse side of the edge, see Figure 4(b) for an example. The last property of Lemma 5.2 still applies to orthogonal diagrams. In fact, the face labels fit the pattern

$$z, \bar{z}, \tau(z), \overline{\tau(z)}, \tau^2(z), \dots, \overline{\tau^f(z)},$$

independently of the direction chosen for the boundary. This is because $\tau(\overline{\tau(z)}) = \bar{z}$ due to Lemma 4.10.

Given an orthogonal diagram, we can read off the target permutation in the following fashion. To determine $\tau(z)$, we find the leaf labelled z and go from it along the boundary segment marked solid, until we arrive at the next leaf (which must be marked \bar{z} , according to Def. 5.1). From there we follow the dashed boundary segment. The leaf we arrive at is the leaf $\tau(z)$. Note that the same prescription applies to unitary diagrams as well, if we let z be the labels $\{1, \dots, t\}$ only.

6.2. Operations on diagrams. The two types of operations for unitary diagrams described in Section 5.2 can be defined for orthogonal diagrams in a similar fashion.

In fact, the operation of contracting an edge is the exactly same. Namely, if we have a vertex of degree 4 with the leaf labelled 1 adjacent to it, we can contract the edge that is opposite the leaf 1.

The generalization of the tying/untying operation is a little more exciting. We can tie *any two* leaves together (that is with or without bars). Before tying, the edges need to be arranged as in Fig. 7; this might require adding a twist to one of them, see Fig. 13.

Lemma 6.2. Consider a diagram with the target permutation τ . If we tie the leaves z_1 and z_2 together, the target permutation of the modified diagram is $(z_1 z_2) \tau(\bar{z}_1 \bar{z}_2)$. Untying a 4-vertex

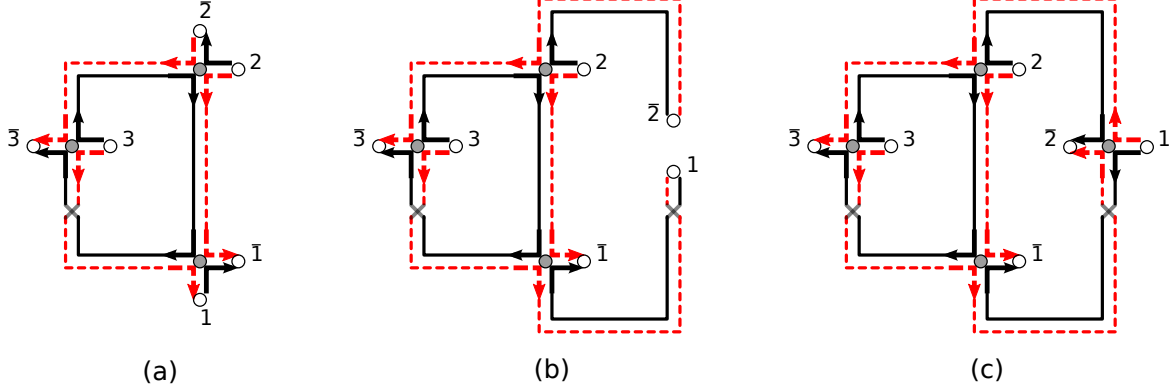


FIGURE 13. An example of tying two leaves in an orthogonal diagram. Part (a) shows the original diagram; leaves 1 and $\bar{2}$ are to be tied. In part (b) one of the edges received a twist to align properly. The result is shown in part (c). According to Lemma 6.2, the target is transformed as $(1\bar{2})(12\bar{3})(3\bar{2}\bar{1})(2\bar{1}) = (123)(\bar{3}\bar{2}\bar{1})$

with leaves z_1 and z_2 directly attached to its opposite sides also results in the target permutation $(z_1 z_2) \tau (\bar{z}_1 \bar{z}_2)$.

Proof. According to the rules of reading off the target permutation, the result of τ is the endpoint of a dashed boundary segment. After tying the leaves, the dashed segment that was finishing at z_1 now finishes at z_2 (see Figure 7) and vice versa. This means that z_1 and z_2 must be switched after the original τ is applied.

Similarly, the image of \bar{z}_1 is computed by following the solid segment to z_1 and then the dashed segment to the leaf that is the result $\tau(\bar{z}_1)$. After the tying operation, the dashed segment coming out of z_1 is actually the segment that was previously coming out of z_2 and therefore leading to $\tau(\bar{z}_2)$. To account for this change, we need to switch \bar{z}_1 and \bar{z}_2 before we apply τ .

The untying operation is equivalent to multiplying by the inverses of the transpositions, which are the transpositions themselves. \square

Remark 6.3. The operation $(z_1 z_2) \tau (\bar{z}_1 \bar{z}_2) =: \tilde{\tau}$ preserves the properties described in Lemma 4.10. Indeed, according to Remark 4.11, we need to show that $T\tilde{\tau}$ consists only of cycles of length 2. Denoting $(\bar{z}_1 \bar{z}_2) =: q$, we have $(z_1 z_2) = TqT$ and therefore $T\tilde{\tau} = TTqT\tau q = qT\tau q \sim T\tau$. Since the operation of conjugation does not affect the cycle type, $T\tilde{\tau}$ has the same cycle lengths as $T\tau$.

6.3. Cancellations among the orthogonal diagrams. Similarly to the unitary case, comparing Lemma 4.14 with the RMT result (7), we see that we need to compare the coefficients $\Delta^0(\tau)$ and $V_N^0(\varpi)$ (where $\tau = \varpi^{-1}T\varpi T$). Moreover, according to Lemma 4.13, both coefficients in fact depend on the set of numbers c_1, \dots, c_k , which are the lengths of half the cycles in the cycle representation of τ (each cycle has its “mirror” image in the representation, see Lemma 4.10; only one length per pair appears in the list).

The coefficient $\Delta^O(\tau)$ is the sum of contributions of orthogonal diagrams with the target permutation τ . The contribution of every diagram is evaluated according to the rules in Definition 3.1. Denoting by $D_{v,e}^O(\tau)$ the number of orthogonal diagrams with the target permutation τ , v internal vertices and e edges, we have the following statement.

Theorem 6.4. *The total contribution of the orthogonal diagrams with target permutation τ is*

$$(28) \quad \Delta^O(\tau) := \sum_{v,e} D_{v,e}^O(\tau) \frac{(-1)^v}{N^{e-v}} = V_N^O(\tau).$$

Proof. The cancellation algorithm is completely analogous to the unitary case. Namely, we fix a linear ordering of the set Z_t and untie, while it is possible, the vertex adjacent to the leaf with the minimal label of the leaves still present in the diagram. We remove any edges that directly connect two leaves from the consideration.

If at any point it becomes impossible to untie the vertex adjacent to the minimal leaf, it is either because the vertex is of a degree higher than 4 or because the edge opposite the minimal leaf is not going to a leaf. Then we correspondingly split the vertex or contract the edge. After this we re-tie previously untied vertices. The new diagram has the contribution that cancels the contribution of the original diagram.

The only diagrams that survive this process are those that untie to an empty diagram. Recording every step according to Lemma 6.2, we get

$$(29) \quad (s_v r_v) \cdots (s_2 r_2) (s_1 r_1) \tau (\overline{s_1 r_1}) (\overline{s_2 r_2}) \cdots (\overline{s_v r_v}) = id,$$

where $s_j < r_j$ and $s_j \leq s_{j+1}$. Note that the choice of the node to untie is unique at each step, so the surviving diagrams are in one-to-one correspondence with the ‘‘palindromic’’ primitive factorizations

$$(30) \quad \tau = (s_1 r_1) (s_2 r_2) \cdots (s_v r_v) (\overline{s_v r_v}) \cdots (\overline{s_2 r_2}) (\overline{s_1 r_1}), \quad s_j < r_j, \quad s_j \leq s_{j+1}.$$

We now need to understand the number $p_v^O(\tau) = p_v^O(c_1, \dots, c_k)$ of such factorizations which provide us with the semiclassical contribution.

$$(31) \quad \Delta^O(\tau) := \sum_v p_v^O(\tau) \frac{(-1)^v}{N^{e-v}}.$$

To do this, we derive a recursion similar to (26). The number of factorizations of τ with $2v$ factors is equal to the number of factorization of $(s_1 r_1) \tau (\overline{s_1 r_1})$ with $2(v-1)$ factors, summed over all possible choices of $(s_1 r_1)$. As before, we treat the case $s_1 \neq \min(Z_t)$ separately (s_1 and $\overline{s_1}$ must then be cycles of their own).

Without loss of generality we assume that s_1 appears in cycle number 1. There are $2c_j$ possibilities for r_1 to appear in the cycle number $j > 1$ or its ‘‘mirror’’ image, cycle number $2k - j + 1$. This cycle joins the first cycle in the result of the multiplication $(s_1 r_1) \tau (\overline{s_1 r_1})$. If r_1 belongs to the first cycle, it splits into two parts. Finally, if r_1 belongs to the mirror image of the first cycle, the product is

$$(s_1 r_1) (s_1 a \dots b \overline{r_1} c \dots d) (\overline{d} \dots \overline{c} r_1 \overline{b} \dots \overline{a} \overline{s_1}) (\overline{r_1} \overline{s_1}) = (s_1 a \dots b \overline{r_1} \overline{d} \dots \overline{c}) (c \dots d r_1 \overline{b} \dots \overline{a} \overline{s_1}),$$

therefore the cycle lengths do not change. In the latter case, r_1 has c_1 possibilities, including $\overline{s_1}$.

The cases above give rise to the following terms,

$$(32) \quad p_v^{\text{O}}(c_1, \dots, c_k) = \delta_{c_1, 1} p_v^{\text{O}}(c_2, \dots, c_k) + \sum_j 2c_j p_{v-1}^{\text{O}}(c_1 + c_j, \dots, \hat{c}_j, \dots) \\ + \sum_{q+r=c_1} p_{v-1}^{\text{O}}(q, r, c_2, \dots, c_k) + c_1 p_{v-1}^{\text{O}}(c_1, \dots, c_k).$$

Taking the generating function with respect to $1/N$ according to the middle expression in (28), we recover recursion (10), which completes the proof. \square

7. CONCLUSIONS

While the RMT approach described in Sec. 2 in terms of the recursive class coefficients is computationally inefficient, it turned out to be useful for establishing the equivalence between semiclassics and RMT to all orders of $1/N$. The equivalence is established at the level of moments of scattering matrix elements which immediately implies equivalence of moments (both linear and non-linear) of matrix subblocks. The result is proved for moments of COE and CUE (corresp. with and without time-reversal symmetry), but, since there is a simple formula [15] connecting COE and CSE moments, the equivalence extends immediately to CSE moments (corresp. systems with spin-orbit interactions) as well.

Furthermore, since all the moments agree, indirectly we obtain the joint probability density of the transmission eigenvalues of $\mathbf{t}^\dagger \mathbf{t}$ semiclassically. In fact, current RMT approaches start from this joint probability density (which follows the Jacobi ensemble [2, 21]) and obtain linear and non-linear transport moments through a variety of different methods [28, 34, 42, 44, 53, 57, 58, 63, 64, 74].

Once the semiclassical diagrams have been expressed in terms of ribbon graphs, the most important step is showing that the contributions of the vast majority of diagrams cancel. We identified pairs of diagrams whose contributions cancel exactly, leaving only the diagrams that correspond to primitive factorisations. These were then shown to match the RMT class coefficients. While possibly the simplest cancellation algorithm, it is certainly not unique. In fact, in an earlier version of our proof we considered a cancellation algorithm which reduced the set of diagrams (with broken TRS) to those that can be put into correspondence with inequivalent factorisations [5] (those are the fully untieable diagrams, when more general untyings are allowed).

The cancellation we used relies strongly on the product of the semiclassical edge and vertex contribution from Definition 3.1 being exactly -1 . This is the case for the correlators of the subblocks of the scattering matrix we considered here, but no longer holds for energy-dependent correlators, superconducting or tunneling leads, Wigner delay times and other physically relevant questions. In these cases semiclassical results are known for low moments or up to a given order in inverse channel number [6, 7, 31, 29, 30] and agree with perturbative RMT expansions [3, 15, 16, 40, 41, 43, 70] but a general proof of the equivalence is lacking. For the Wigner delay times, the transport matrix follows an inverse Wishart distribution [16] and correlators of such matrices have been expressed [35] in a form similar to the correlators in Sec. 2. A strategy similar to the one used here might then be fruitful. Starting from the joint probability density of the delay times, the linear moments, as well as the moments of the mean time delay, are also available from RMT [34, 42, 44].

Another case where the edge and vertex contributions do not allow direct cancellation is when we consider Ehrenfest time effects. Below the Ehrenfest time the quantum and classical propagation are fairly similar while for longer times wave interference dominates. This wave interference is incorporated in the semiclassical approximation on top of the underlying classical motion which can then be used to obtain the typical dependence of quantum transport on the Ehrenfest time. In particular results are known for low orders in a perturbative expansion in the inverse channel number for low moments [17, 18, 27, 59, 75, 76, 79, 80] and for all moments at leading order [77]. Although this question is outside the range of applicability of RMT, attempts have been made to phenomenologically treat Ehrenfest time effects using “effective” RMT [67, 68]. This approach provides the correct results for some quantities but importantly not for all (notably the weak localisation correction to the conductance) and its validity must then be checked against semiclassical approaches [18, 27, 77]. It is here, where RMT answers are not available in principle, that our classification of the semiclassical diagrams (continued in [9]) can become very useful.

ACKNOWLEDGEMENTS

Illuminating discussions with J. Irving and K. Richter are gratefully acknowledged. GB is partially supported by the NSF grant DMS-0907968 and JK by the DFG through FOR 760.

REFERENCES

- [1] H. U. Baranger, R. A. Jalabert, and A. D. Stone. Weak localization and integrability in ballistic cavities. *Phys. Rev. Lett.*, 70:3876–3879, 1993.
- [2] C. W. J. Beenakker. Random-matrix theory of quantum transport. *Rev. Mod. Phys.*, 69:731–808, 1997.
- [3] C. W. J. Beenakker, J. A. Melsen, and P. W. Brouwer. Giant backscattering peak in angle-resolved Andreev reflection. *Phys. Rev. B*, 51:13883–13886, 1995.
- [4] G. Berkolaiko, J. M. Harrison, and M. Novaes. Full counting statistics of chaotic cavities from classical action correlations. *J. Phys. A*, 41:365102, 2008.
- [5] G. Berkolaiko and J. Irving. Inequivalent transitive factorizations of permutations into transpositions. In preparation, 2013.
- [6] G. Berkolaiko and J. Kuipers. Moments of the Wigner delay times. *J. Phys. A*, 43:035101, 2010.
- [7] G. Berkolaiko and J. Kuipers. Transport moments beyond the leading order. *New J. Phys.*, 13:063020, 2011.
- [8] G. Berkolaiko and J. Kuipers. Universality in chaotic quantum transport: The concordance between random matrix and semiclassical theories. *Phys. Rev. E*, 85:045201, 2012.
- [9] G. Berkolaiko and J. Kuipers. Combinatorial theory of the semiclassical evaluation of transport moments II. preprint [arXiv:1307.3280](https://arxiv.org/abs/1307.3280), 2013.
- [10] G. Berkolaiko, H. Schanz, and R. S. Whitney. Form factor for a family of quantum graphs: an expansion to third order. *Journal of Physics A: Mathematical and General*, 36(31):8373, 2003.
- [11] M. V. Berry. Semiclassical theory of spectral rigidity. *Proc. Roy. Soc. A*, 400:229–251, 1985.
- [12] R. Blümel and U. Smilansky. Classical irregular scattering and its quantum-mechanical implications. *Phys. Rev. Lett.*, 60:477–480, 1988.
- [13] R. Blümel and U. Smilansky. Random-matrix description of chaotic scattering: Semiclassical approach. *Phys. Rev. Lett.*, 64:241–244, 1990.
- [14] P. Braun, S. Heusler, S. Müller, and F. Haake. Semiclassical prediction for shot noise in chaotic cavities. *J. Phys. A*, 39:L159–L165, 2006.
- [15] P. W. Brouwer and C. W. J. Beenakker. Diagrammatic method of integration over the unitary group, with applications to quantum transport in mesoscopic systems. *J. Math. Phys.*, 37:4904–4934, 1996.
- [16] P. W. Brouwer, K. M. Frahm, and C. W. J. Beenakker. Distribution of the quantum mechanical time-delay matrix for a chaotic cavity. *Waves in Random Media*, 9:91–104, 1999.
- [17] P. W. Brouwer and S. Rahav. Semiclassical theory of the Ehrenfest time dependence of quantum transport in ballistic quantum dots. *Phys. Rev. B*, 74:075322, 2006.

- [18] P. W. Brouwer and S. Rahav. Towards a semiclassical justification of the effective random matrix theory for transport through ballistic quantum dots. *Phys. Rev. B*, 74:085313, 2006.
- [19] M. Büttiker. Four-terminal phase-coherent conductance. *Phys. Rev. Lett.*, 57:1761–1764, 1986.
- [20] B. Collins. Moments and cumulants of polynomial random variables on unitary groups, the Itzykson-Zuber integral, and free probability. *Int. Math. Res. Not.*, 2003:953–982, 2003.
- [21] P. J. Forrester. Quantum conductance problems and the Jacobi ensemble. *J. Phys. A*, 39:6861–6870, 2006.
- [22] I. Goulden, M. Guay-Paquet, and J. Novak. Monotone Hurwitz numbers and the HCIZ integral II. Preprint [arXiv:1107.1001](https://arxiv.org/abs/1107.1001), 2011.
- [23] J. H. Hannay and A. M. Ozorio de Almeida. Periodic orbits and a correlation function for the semiclassical density of states. *J. Phys. A*, 17:3429–3440, 1984.
- [24] S. Heusler, S. Müller, A. Altland, P. Braun, and F. Haake. Periodic-orbit theory of level correlations. *Phys. Rev. Lett.*, 98:044103, 2007.
- [25] S. Heusler, S. Müller, P. Braun, and F. Haake. Semiclassical theory of chaotic conductors. *Phys. Rev. Lett.*, 96:066804, 2006.
- [26] D. M. Jackson and T. I. Visentin. *An atlas of the smaller maps in orientable and nonorientable surfaces*. CRC Press Series on Discrete Mathematics and its Applications. Chapman & Hall/CRC, Boca Raton, FL, 2001.
- [27] Ph. Jacquod and R. S. Whitney. Semiclassical theory of quantum chaotic transport: Phase-space splitting, coherent backscattering and weak localization. *Phys. Rev. B*, 73:195115, 2006.
- [28] B. A. Khoruzhenko, D. V. Savin, and H.-J. Sommers. Systematic approach to statistics of conductance and shot-noise in chaotic cavities. *Phys. Rev. B*, 80:125301, 2009.
- [29] J. Kuipers, T. Engl, G. Berkolaiko, C. Petitjean, D. Waltner, and K. Richter. The density of states of chaotic Andreev billiards. *Phys. Rev. B*, 83:195316, 2011.
- [30] J. Kuipers and K. Richter. Transport moments and Andreev billiards with tunnel barriers. *J. Phys. A*, 46:055101, 2013.
- [31] J. Kuipers, D. Waltner, C. Petitjean, G. Berkolaiko, and K. Richter. Semiclassical gaps in the density of states of chaotic Andreev billiards. *Phys. Rev. Lett.*, 104:027001, 2010.
- [32] R. Landauer. Spatial variation of currents and fields due to localized scatterers in metallic conduction. *IBM J. Res. Dev.*, 1:223–231, 1957.
- [33] R. Landauer. Spatial variation of currents and fields due to localized scatterers in metallic conduction. *IBM J. Res. Dev.*, 33:306–316, 1988.
- [34] G. Livan and P. Vivo. Moments of Wishart-Laguerre and Jacobi ensembles of random matrices: Application to the quantum transport problem in chaotic cavities. *Acta Phys. Pol. B*, 42:1081–1104, 2011.
- [35] S. Matsumoto. General moments of the inverse real Wishart distribution and orthogonal Weingarten functions. *J. Theor. Prob.*, 25:798–822, 2012.
- [36] S. Matsumoto. Weingarten calculus for matrix ensembles associated with compact symmetric spaces. *Random Matrices: Theory Appl.*, 2:1350001, 2013.
- [37] S. Matsumoto and J. Novak. Unitary matrix integrals, primitive factorizations, and Jucys-Murphy elements. In *22nd International Conference on Formal Power Series and Algebraic Combinatorics (FPSAC 2010)*, pages 403–412. DMTCS Proceedings, 2010.
- [38] P. A. Mello. Averages on the unitary group and applications to the problem of disordered conductors. *J. Phys. A*, 23:4061–4080, 1990.
- [39] P. A. Mello and T. H. Seligman. On the entropy approach to statistical nuclear reactions. *Nuc. Phys. A*, 344:489–508, 1980.
- [40] J. A. Melsen, P. W. Brouwer, K. M. Frahm, and C. W. J. Beenakker. Induced superconductivity distinguishes chaotic from integrable billiards. *Europhys. Lett.*, 35:7–12, 1996.
- [41] J. A. Melsen, P. W. Brouwer, K. M. Frahm, and C. W. J. Beenakker. Superconductor-proximity effect in chaotic and integrable billiards. *Phys. Scr.*, T69:223–225, 1997.
- [42] F. Mezzadri and N. Simm. Moments of the transmission eigenvalues, proper delay times and random matrix theory I. *J. Math. Phys.*, 52:103511, 2011.
- [43] F. Mezzadri and N. Simm. Moments of the transmission eigenvalues, proper delay times and random matrix theory II. *J. Math. Phys.*, 53:053504, 2012.
- [44] F. Mezzadri and N. Simm. Tau-function theory of quantum chaotic transport with $\beta=1,2,4$. Preprint [arXiv:1206.4584](https://arxiv.org/abs/1206.4584), 2012.

- [45] W. H. Miller. The classical S-matrix in molecular collisions. *Adv. Chem. Phys.*, 30:77–136, 1975.
- [46] S. Müller, S. Heusler, A. Altland, P. Braun, and F. Haake. Periodic-orbit theory of universal level correlations in quantum chaos. *New J. Phys.*, 11:103025, 2009.
- [47] S. Müller, S. Heusler, P. Braun, and F. Haake. Semiclassical approach to chaotic quantum transport. *New J. Phys.*, 9:12, 2007.
- [48] S. Müller, S. Heusler, P. Braun, F. Haake, and A. Altland. Semiclassical foundation of universality in quantum chaos. *Phys. Rev. Lett.*, 93:014103, 2004.
- [49] S. Müller, S. Heusler, P. Braun, F. Haake, and A. Altland. Periodic-orbit theory of universality in quantum chaos. *Phys. Rev. E*, 72:046207, 2005.
- [50] Another name present in the literature is “Weingarten” function [78], even though it was probably Samuel [62] who first defined the function and systematically studied it.
- [51] Thus, despite the word “orthogonal” in the name, it is not the orthogonal group $O(N)$. Rather, it can be identified with $U(N)/O(N)$.
- [52] The traditional definitions are slightly different from ours in ordering the second elements of the transpositions.
- [53] M. Novaes. Statistics of quantum transport in chaotic cavities with broken time-reversal symmetry. *Phys. Rev. B*, 78:035337, 2008.
- [54] M. Novaes. Semiclassical approach to universality in quantum chaotic transport. *EPL*, 98:20006, 2012.
- [55] M. Novaes. Combinatorial problems in the semiclassical approach to quantum chaotic transport. *J. Phys. A*, 46:095101, 2013.
- [56] M. Novaes. A semiclassical matrix model for quantum chaotic transport. Preprint, 2013.
- [57] V. A. Osipov and E. Kanzieper. Integrable theory of quantum transport in chaotic cavities. *Phys. Rev. Lett.*, 101:176804, 2008.
- [58] V. A. Osipov and E. Kanzieper. Statistics of thermal to shot noise crossover in chaotic cavities. *J. Phys. A*, 42:475101, 2009.
- [59] C. Petitjean, D. Waltner, J. Kuipers, I. Adagideli, and K. Richter. Semiclassical approach to the dynamical conductance of a chaotic cavity. *Phys. Rev. B*, 80:115310, 2009.
- [60] K. Richter. *Semiclassical theory of mesoscopic quantum systems*. Springer, Berlin, 2000.
- [61] K. Richter and M. Sieber. Semiclassical theory of chaotic quantum transport. *Phys. Rev. Lett.*, 89:206801, 2002.
- [62] S. Samuel. $U(N)$ integrals, $1/N$, and the De Wit-’t Hooft anomalies. *J. Math. Phys.*, 21:2695–2703, 1980.
- [63] D. V. Savin and H.-J. Sommers. Shot noise in chaotic cavities with an arbitrary number of open channels. *Phys. Rev. B*, 73:081307, 2006.
- [64] D. V. Savin, H.-J. Sommers, and W. Wiczeorek. Nonlinear statistics of quantum transport in chaotic cavities. *Phys. Rev. B*, 77:125332, 2008.
- [65] M. Sieber. Leading off-diagonal approximation for the spectral form factor for uniformly hyperbolic systems. *J. Phys. A*, 35:L613–L619, 2002.
- [66] M. Sieber and K. Richter. Correlations between periodic orbits and their rôle in spectral statistics. *Phys. Scr.*, T90:128–133, 2001.
- [67] P. G. Silvestrov, M. C. Goorden, and C. W. J. Beenakker. Adiabatic quantization of Andreev quantum billiard levels. *Phys. Rev. Lett.*, 90:116801, 2003.
- [68] P. G. Silvestrov, M. C. Goorden, and C. W. J. Beenakker. Noiseless scattering states in a chaotic cavity. *Phys. Rev. B*, 67:241301, 2003.
- [69] R. A. Smith, I. V. Lerner, and B. L. Altshuler. Spectral statistics in disordered metals: A trajectories approach. *Phys. Rev. B*, 58:10343–10350, Oct 1998.
- [70] H.-J. Sommers, D. V. Savin, and V. V. Sokolov. Distribution of proper delay times in quantum chaotic scattering: A crossover from ideal to weak coupling. *Phys. Rev. Lett.*, 87:094101, 2001.
- [71] D. Spehner. Spectral form factor of hyperbolic systems: leading off-diagonal approximation. *J. Phys. A*, 36(26):7269–7290, 2003.
- [72] M. Turek and K. Richter. Leading off-diagonal contribution to the spectral form factor of chaotic quantum systems. *J. Phys. A-Math. Gen.*, 36(30):L455–L462, 2003.
- [73] W. T. Tutte. *Graph theory*, volume 21 of *Encyclopedia of Mathematics and its Applications*. Addison-Wesley, Reading, MA, 1984.

- [74] P. Vivo and E. Vivo. Transmission eigenvalue densities and moments in chaotic cavities from random matrix theory. *J. Phys. A*, 41:122004, 2008.
- [75] D. Waltner and J. Kuipers. Ehrenfest time dependence of quantum transport corrections and spectral statistics. *Phys. Rev. E*, 82:066205, 2010.
- [76] D. Waltner, J. Kuipers, Ph. Jacquod, and K. Richter. Conductance fluctuations in chaotic systems with tunnel barriers. *Phys. Rev. B*, 85:024302, 2012.
- [77] D. Waltner, J. Kuipers, and K. Richter. Ehrenfest-time dependence of counting statistics for chaotic ballistic systems. *Phys. Rev. B*, 83:195315, 2011.
- [78] D. Weingarten. Asymptotic behavior of group integrals in the limit of infinite rank. *J. Math. Phys.*, 19:999–1001, 1978.
- [79] R. S. Whitney. Suppression of weak localization and enhancement of noise by tunneling in semiclassical chaotic transport. *Phys. Rev. B*, 75:235404, 2007.
- [80] R. S. Whitney and Ph. Jacquod. Shot noise in semiclassical chaotic cavities. *Phys. Rev. Lett.*, 96:206804, 2006.
- [81] A. Zvonkin. Matrix integrals and map enumeration: an accessible introduction. *Math. Comput. Modelling*, 26:281–304, 1997.

DEPARTMENT OF MATHEMATICS, TEXAS A&M UNIVERSITY, COLLEGE STATION, TX 77843-3368, USA
E-mail address: `berko@math.tamu.edu`

INSTITUT FÜR THEORETISCHE PHYSIK, UNIVERSITÄT REGENSBURG, D-93040 REGENSBURG, GERMANY
E-mail address: `Jack.Kuipers@physik.uni-regensburg.de`